Journal of African Earth Sciences 228 (2025) 105664

Contents lists available at ScienceDirect

Journal of African Earth Sciences

journal homepage: www.elsevier.com/locate/jafrearsci

Invited Review

The structure of Precambrian crust in sub-Saharan Africa: An AfricaArray synthesis and review☆

Alexandra Sabattier[a], Andrew Nyblade[a,b,*], Raymond Durrheim[b], Fenitra Andriampenomanana[b], Andriamiranto Raveloson[c], Islam Fadel[d], Mark van der Meijde[d], Amanda Willet[a]

[a] Department of Geosciences, Penn State University, University Park, PA, 16802, USA
[b] School of Geosciences, The University of the Witwatersrand, Johannesburg, South Africa
[c] Institute and Observatory of Geophysics in Antananarivo, Antananarivo, Madagascar
[d] Faculty of Geo-Information Science and Earth Observation (ITC), University of Twente, Enschede, the Netherlands

ARTICLE INFO

Handling editor: DR Damien Delvaux

Keywords:
Sub-Saharan Africa
Precambrian
Crust
Moho depth
Shear wave velocities
Secular variation

ABSTRACT

We combine new estimates of crustal thickness and shear wave velocities from 48 broadband seismic stations in Mozambique, Namibia, South Africa and Uganda with previously published results to review and examine Precambrian crustal structure in sub-Saharan Africa for secular trends. The ensemble of crustal structure estimates used relies heavily on data obtained through the AfricaArray initiative, which is briefly reviewed. Whether or not Precambrian crustal structure exhibits notable changes from the Mesoarchean through the Neoproterozoic places a key constraint on continental crustal genesis and evolution. Our 48 new estimates of Moho depth and crustal shear wave velocity profiles, combined with results from similar previous studies, yield an average crustal thickness for all Precambrian terranes of 39 ± 4 km. We find that average crustal thicknesses are essentially identical for Mesoarchean (38 ± 3 km), Neoarchean (39 ± 4 km), Paleoproterozoic (40 ± 4 km), Mesoproterozoic (40 ± 4 km) and Neoproterozoic (39 ± 4 km) terranes. The average thickness of the mafic lower crust, identified by high velocity layering (Vs > 4.0 km/s), is also almost identical in Archean and Proterozoic terranes (7 ± 4 km and 6 ± 4 km, respectively). Finally, the average crustal shear wave velocities for all terranes fall within 1 standard deviation of a mean velocity of 3.7 km/s. These results are consistent with findings from other studies highlighting a lack of evidence for secular variation in crustal structure or composition within Precambrian terranes in sub-Saharan Africa, suggesting that secular trends, if they existed at the time of crust formation, have been obscured by crustal reworking during later orogenic and/or magmatic events.

1. Introduction

In this paper, we provide a review of Precambrian crustal structure in parts of sub-Saharan Africa that draws heavily on both published and new estimates of Moho depth and crustal shear wave velocities using broadband seismic data obtained through the AfricaArray initiative. As the AfricaArray initiative is central to the results presented, we begin with a short summary of the initiative. Following that, new estimates of crustal thickness and shear wave velocities are presented for 48 seismic stations in Mozambique, Namibia, South Africa and Uganda (Fig. 1) obtained by modelling P-wave receiver functions using the H-κ stacking method (Zhu and Kanamori, 2000) and a joint inversion of receiver functions and Rayleigh wave dispersion measurements (Julia et al., 2000). The new estimates are then combined with published results from other seismic stations in sub-Saharan Africa (Fig. 1) to re-evaluate evidence for secular changes in Precambrian crustal thickness and composition.

The question of whether Precambrian crustal thickness and composition has changed over time has been debated in the literature for several decades, and the answer to that question has direct bearing on understanding crustal genesis and evolution. Some researchers have suggested major differences in crustal structure and composition exist between Archean and Proterozoic terranes (e.g., Abbott et al., 2013; Durrheim and Mooney, 1994; Thompson et al., 2010), pointing to

☆ For submission as a review article to the Journal of African Earth Sciences.

* Corresponding author. Department of Geosciences, Penn State University, University Park, PA, 16802, USA.
E-mail address: aan2@psu.edu (A. Nyblade).

https://doi.org/10.1016/j.jafrearsci.2025.105664
Received 6 December 2024; Received in revised form 4 April 2025; Accepted 8 April 2025
Available online 10 April 2025

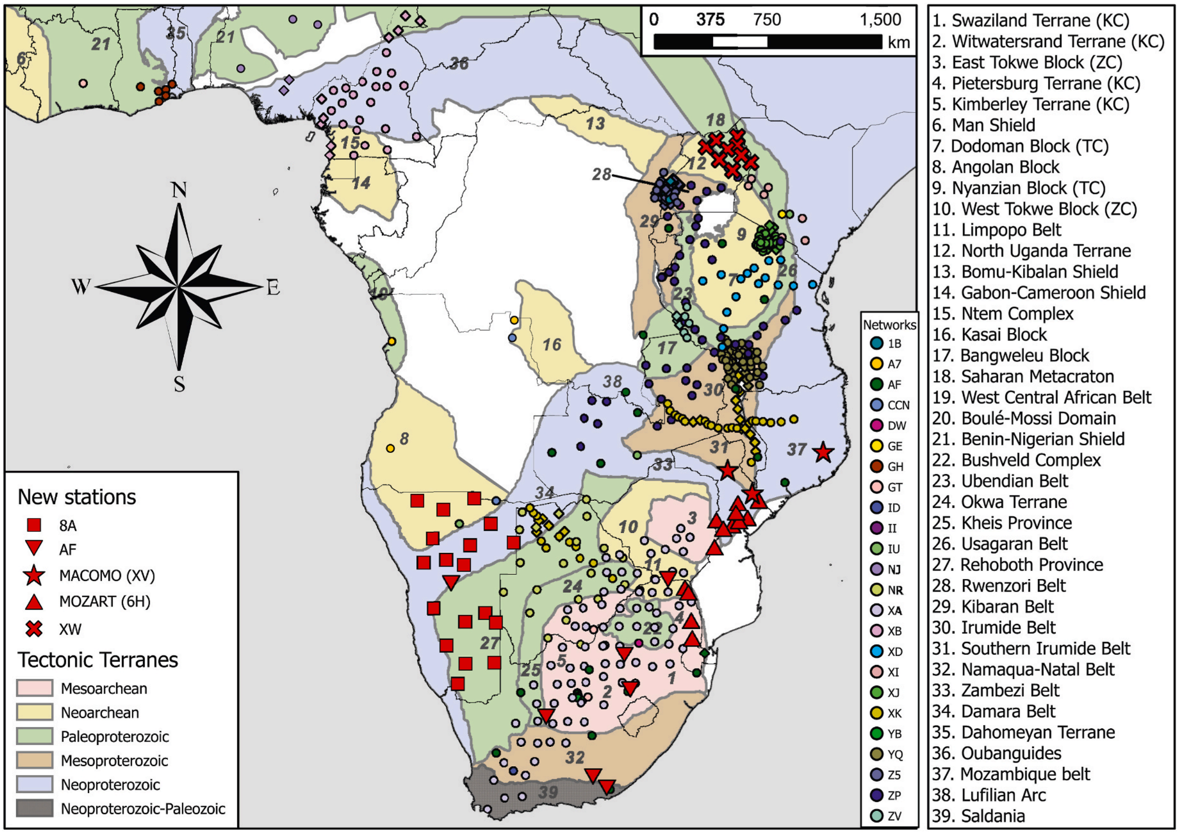

Fig. 1. Precambrian tectonic terranes (modified after Begg et al., 2009; Tugume et al., 2013) and locations of seismic stations used in this study. New stations analysed in this study are displayed in red. Stations from previous studies are color-coded by network. Stations located in Precambrian terranes are displayed as circles; stations located in younger rifts and basin are displayed as diamonds. Terranes are numbered and defined in the map key. KC = Kaapvaal Craton; TC = Tanzania Craton; and ZC = Zimbabwe Craton.

changes in continental crust formation through much of Earth history, while others argue that there are only minimal, if any, differences (e.g., Rudnick and Fountain, 1995; Rudnick and Gao, 2003; Stankiewicz and de Wit, 2013; Zandt and Ammon, 1995), indicating little temporal change in the processes forming continental crust. Results from previous studies in sub-Saharan Africa using the same methodologies as used in this study have provided little evidence for age-related trends in Precambrian crustal structure (Kachingwe et al., 2015; Tugume et al., 2012, 2013), suggesting that secular trends, if they once existed, have been obscured by the tectonic reworking of crustal structure during later orogenic and/or magmatic events. Here we use an expanded ensemble of results on crustal thickness and shear wave velocities to re-examine that finding.

2. AfricaArray

AfricaArray (www.africaarray.net), a multi-faceted education and research capacity building initiative, was started in 2005 as an intervention to rebuild the geophysics program at the University of the Witwatersrand (Wits) in Johannesburg, South Africa. In 2004, the Head of the School of Geosciences, Prof. Paul Dirks, approached Prof. Andrew Nyblade at Penn State University about how to rebuild the once preeminent geophysics program at Wits, which had gone into decline during the 1990's. Together, Nyblade and Dirks formulated a plan containing five key elements: 1) Fund raising to increase the number of geophysics faculty at Wits and support a vigorous research program in solid Earth geophysics; 2) Establishing a geophysical observatory network to provide data for research conducted by faculty, students and postdocs; 3) Expand the geophysics field school at Wits, which was part of the B.Sc. Honours degree in geophysics, to include students from other universities; 4) Hold an annual science workshop to help create community and provide a venue for sharing scientific results; 5) Develop programs to attract students to Wits from historically disadvantaged communities (Nyblade et al., 2008). Nyblade, aware that in the U.S. there were similar issues of underrepresentation in the geosciences, added a sixth element, a diversity program for U.S. students at Penn State that linked to programs at Wits to provide an international educational experience for U.S. underrepresented minority students.

After a year of successful fundraising and the Council for Geoscience (aka South African Geological Survey) pledging ten seismic stations from the South African National Seismic Network to start the geophysical observatory network, AfricaArray was launched in 2005 with an inaugural workshop at Wits. The workshop was attended by geoscientists from throughout Africa, and because of the needs expressed at that workshop for improved science capacity building elsewhere in Africa, a decision was made to expand the geophysical observatory network beyond South Africa, and, where possible, support research and the training of African students at other African universities. AfricaArray grew quickly, with seismic observatories established in many African countries, participation in the geophysics field school by students from outside Wits, and the development of industry collaborations. In 2007, Ray Durrheim was hired into a chaired professor position at Wits with support from the South African National Research Foundation, and with Durrheim on board, the number of AfricaArray graduate students and postdocs at Wits expanded rapidly. In 2009, Dirks left Wits for a faculty position in Australia, and Durrheim took over as co-director of AfricaArray with Nyblade. By 2010, the observatory network had expanded of over 50 seismic stations in more than 15 African countries, and in 2011–2012 GPS receivers and automated weather stations were added to about half the observatories (Nyblade et al., 2011; Durrheim and

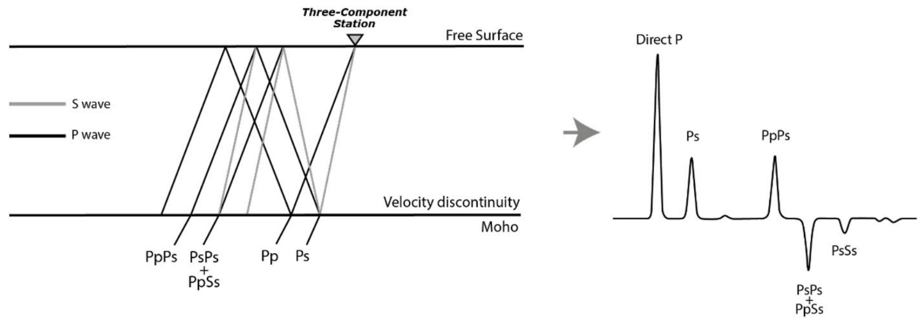

Fig. 2. (Left) Simplified diagram illustrating the major P-to-S converted phases comprising a P-wave receiver function for a single layer over a half space. (Right) The synthetic radial receiver function (waveform) corresponding to the model. Modified from Ammon et al. (1990).

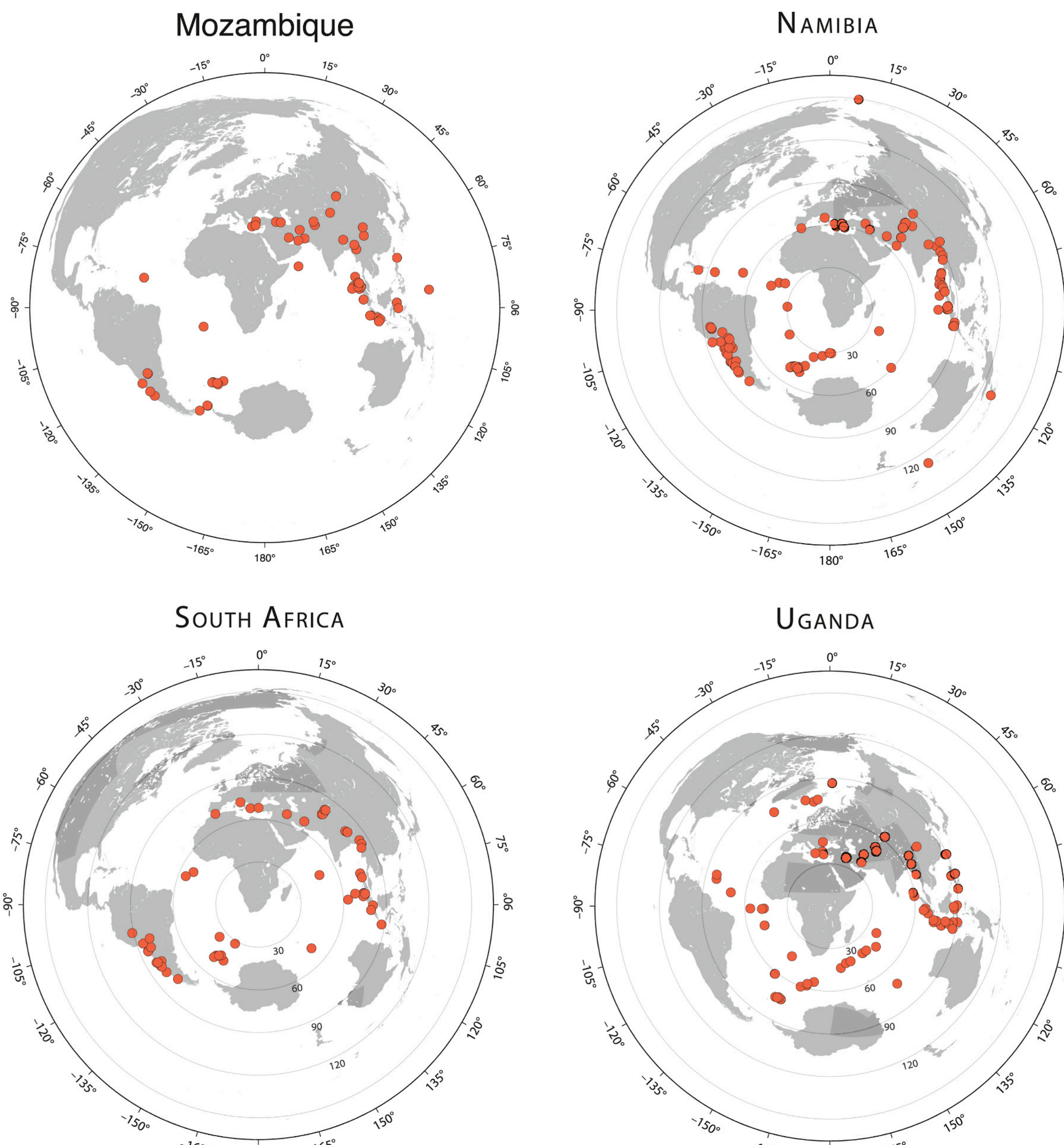

Fig. 3. Map showing the earthquake distribution for the events (red dots) used in this study. The maps are centred around each of the countries studied. Circles on the maps represent the epicentral distances in degrees.

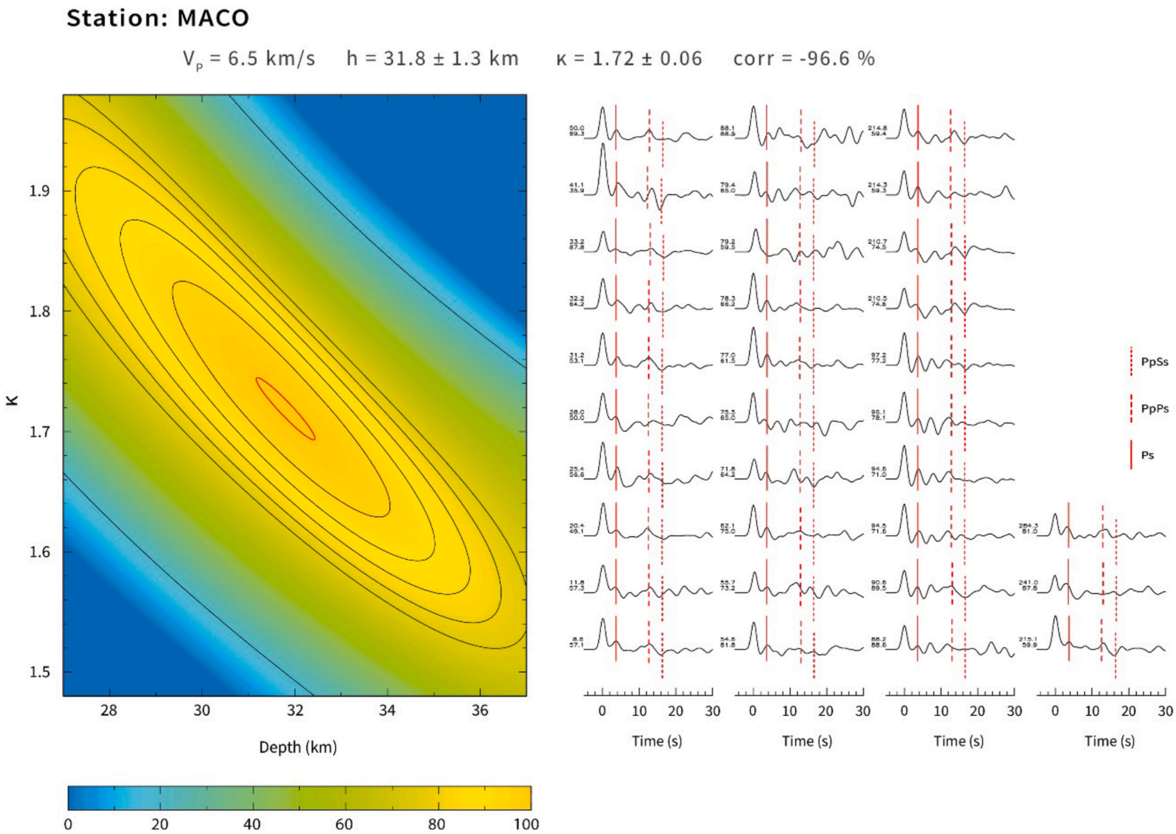

Fig. 4. H-κ results for station MACO. The H-κ parameter space is displayed on the left panel. A red ellipse indicates the 95 % confidence bound and the black contours indicate the fit to S(H, κ) at 10 % intervals. Optimal values for H (Moho depth) and κ (Vp/Vs) are displayed at the top together with their uncertainties. The numbers to the left of the waveforms located on the right panel give back azimuth (top number) and epicentral distance (bottom number) in degrees.

Nyblade, 2022).

Over the years, AfricaArray evolved around a number of core components, as originally envisioned by Dirks and Nyblade. The first was an annual science workshop held at Wits University, routinely attended by 80–100 scientists, mostly from Africa, but also from other continents. The workshop served to bring the AfricaArray community together to share science results, network, provide students and postdocs with opportunities for giving public presentations, and for station operators to troubleshoot and solve problems and fix equipment. As the geophysical observatory developed throughout eastern, western and southern Africa, it provided an increasing volume of open-access data, archived under the AF network code at the IRIS data management center (https://doi.org/10.7914/SN/AF), greatly expanding the availability of broadband seismic data to support research. In addition, many project-specific temporary seismic networks were deployed for one or more years in several countries. The geophysics field school, run annually over a 2-week period, provided students from all over Africa a unique opportunity to build friendships and collaborations while at the same time gain valuable training in practical geophysical data acquisition, processing and interpretation methods (Webb et al., 2015). The final, and perhaps most important core component, was the training of undergraduate and postgraduate students at Wits, Penn State and several other African universities. Between receiving degrees (B.Sc. Honours, M. S., Ph.D.), attending the field school and workshops, and participating in the U.S. diversity program, well over 200 students were part of the AfricaArray initiative between 2005 and 2024.

Today, AfricaArray remains a vital part of the School of Geosciences at Wits. Although the permanent observatory network was shut down during the covid-19 pandemic and has not yet been restarted, the research and education program at Wits in 2025 is going strong, with over 40 postgraduate students and postdocs supported. In 2022, Durrheim retired, and Prof. Musa Manzi, who was a student in the AfricaArray initiative from 2008 to 2013, took on the role of co-director. Besides Mazi, the AfricaArray program at Wits is supported by Prof. Sue Webb and Dr. Stephanie Scheiber-Enslin.

The scientific impact of the AfricaArray initiative can be measured not only by the many new seismic and other geophysical data sets acquired through the initiative, but more importantly by the many faculty, students and postdocs who have participated in and contributed to AfricaArray research projects, training courses, and scientific meetings, and who have authored/co-authored numerous journal publications on African crust and mantle structure, the tectonic evolution of the African continent, seismotectonics and seismic hazards of sub-Saharan Africa, mine seismology, reflection seismic imaging at basin and sub-basin scale, and potential field imaging. Many of the publications stem from over 100 M.Sc. and Ph.D. theses, and also from research completed by postdocs.

3. Overview of tectonic framework

The Precambrian lithospheric structure of Africa consists of an amalgamation of terranes, including several Archean cratons, stitched together by Proterozoic orogenic belts (Begg et al., 2009). Proterozoic orogenic systems separate the Precambrian tectonic framework of the continent into six major regions cored by Archean cratons: the Kalahari Craton in southern Africa, the Congo Craton in central Africa, the Tanzania Craton in eastern Africa, the West African Craton in northwestern Africa, the East Saharan Craton in north-central Africa, and the Arabian-Nubian Shield in northeastern Africa (Goodwin, 1996). Phanerozoic tectonism has modified both Archean and Proterozoic terranes in many places. Below we review the Precambrian tectonic framework within the region of sub-Saharan Africa shown in Fig. 1.

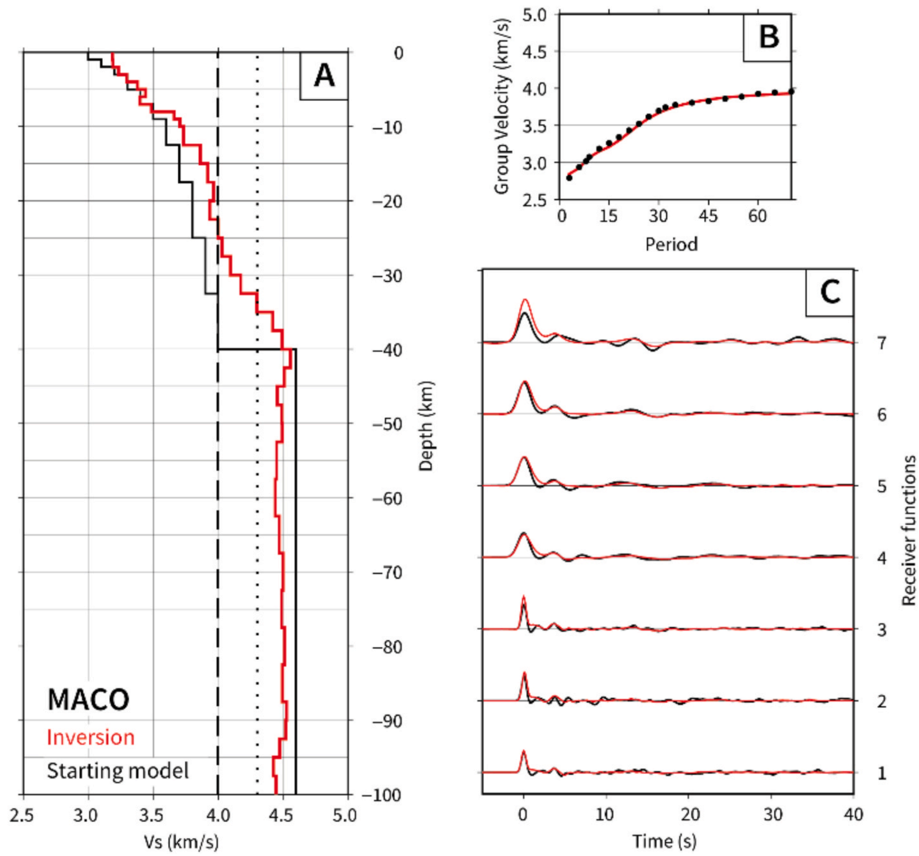

Fig. 5. Results of the joint inversion method for station MACO. **A**. 1-D shear wave velocity model is displayed on the left, showing the starting model (black) and the predicted model (red). The dashed line at ~4.0 km/s and the dotted line at ~4.3 km/s are shown for reference. **B**. Observed (black dots) and predicted (red line) Rayleigh wave group velocities. **C**. Observed and predicted (black and red lines, respectively) receiver function stacks.

3.1. Southern Africa

The Archean Kalahari Craton consists of the Zimbabwe Craton to the north and the Kaapvaal Craton to the south, fused by the 2.6 Ga Limpopo Belt (Dirks et al., 2009; Nguuri et al., 2001) (Fig. 1). The Kaapvaal Craton originated from an early nucleus and predominantly consists of granitoids, gneisses, and greenstone belts formed 3.7–2.7 Ga (Begg et al., 2009; de Wit et al., 1992). It can be divided into several sub-terranes, which include the Kimberley (3.0–2.8 Ga), Pietersburg (3.0–2.8 Ga), Witwatersrand (3.6–3.1 Ga), and Swaziland (3.6–3.2 Ga) blocks separated by the Thabazimbi-Murchison and Colesberg lineaments and the Inyoka fault (Begg et al., 2009; de Wit et al., 1992; Eglington and Armstrong, 2004). The Mesoproterozoic Namaqua–Natal Belt and Paleoproterozoic Kheis Province formed on the craton's southern and western margins, respectively. The Paleoproterozoic Rehoboth Province lies west of the Kheis Province. Trending northeast-southwest along the northwestern boundary of the Kalahari Craton and separating it from the Congo Craton is the Neoproterozoic Damara Mobile Belt, which underwent significant deformation during the Pan African Orogeny (Begg et al., 2009).

Like the Kaapvaal Craton, the 3.6–2.4 Ga Zimbabwe Craton consists of several terranes (Fig. 1). The central gneissic nucleus, the East Tokwe Block, formed between 3.6 and 3.3 Ga. After it stabilized, stable shelf sediments accreted against its western margin (~3.0 Ga), creating the West Tokwe Block. Tectono-magmatic events added granite and greenstones to the West Tokwe Block, as well as clastic and deep-water sediments between 2.7 and 2.6 Ga (Begg et al., 2009; Dirks et al., 2009). This was followed by the emplacement of the Great Dyke layered mafic complex at 2.58 Ga (Begg et al., 2009; Jelsma and Dirks, 2002). On its western margin lies the Paleoprotoerozic Okwa Belt, which is made up of 2.2 Ga low-to-medium grade metamorphic rocks intruded by ~1.9–1.8 Ga granites.

3.2. Eastern Africa

The tectonic framework of eastern Africa is cored by the Archean Tanzania Craton, which is made up of two blocks (Fig. 1). To the north, the Nyanzian Block is comprised of 2.8–2.6 Ga greenstone belts and granites overlaying a molasse and intruded by 2.6 Ga granitoids (Borg and Krogh, 1999). To the south, the Dodoman Block is made up of 2.9–2.8 Ga granodiorites, granitic gneisses, migmatites, as well as other high-grade metamorphic rocks (Borg and Shackleton, 1997; Manya and Maboko, 2003). The Tanzania Craton is surrounded to the south and southeast by the Paleoproterozoic Ubendian and Usagaran Belts. The former contains granulite and amphibole facies gneisses, and metasediments (2.0–1.9 Ga) (Lenoir et al., 1994). Meanwhile, the latter mainly consists of granites, metamorphosed supracrustal rocks, and reworked granitoids (1.9–1.8 Ga) (Möller et al., 1995; Ring et al., 1997). The Mesoproterozoic Kibaran Belt, along the Tanzania Craton's western margin, is largely comprised of amphibolite grade rocks dating back to the Kibaran Orogeny (1.4 Ga) and intruded by 1.4–1.0 Ga granite and granitoids (Kokonyangi et al., 2004; Tack et al., 1994). To the northeast lies the Paleoproterozoic Rwenzori Belt, which is made up of 1.9–1.8 Ga volcanic metasediments (Begg et al., 2009).

The Paleoproterozoic Bangweulu Block is situated to the southwest of the Tanzania Craton and is composed of 2.7 Ga metavolcanic and granitic crystalline rocks intruding into schist belt crystalline basement, reworked during the Paleoproterozoic (De Waele, 2005; De Waele et al., 2006a, 2006b, 2008). Southeast of the Bangweulu Block is the Mesoproterozoic Irumide Belt, consisting of granitoid gneisses and a 1.9 Ga

Table 1
New crustal structure results for the stations used in this study.

Tectonic Province	Station	C	Lat (°)	Long (°)	NC	n	Depth[1] (km)	Vp/Vs	Depth[2] km)	MLC (km)	Avg. Vs (km/s)
Angolan Block	HAO	NA	−17.89	15.06	8A	20	41 ± 2	1.78	40	2.5	3.8
	NEPA	NA	−17.77	18.46	8A	21	41 ± 1	1.85	40	2.5	3.7
	OMUT	NA	−18.41	16.64	8A	40	40 ± 1	1.81	40	2.5	3.7
	OTJO	NA	−20.02	15.98	8A	33	36 ± 1	1.77	38	2.5	3.7
	Ave.						**40**		**39**	**2.5**	**3.7**
Damara Belt	BAHE	NA	−21.35	15.44	8A	35	39 ± 1	1.77	40	2.5	3.8
	GAMM	NA	−20.25	20.83	8A	26	49 ± 1	1.76	48	5	3.7
	HOCH	NA	−21.49	17.85	8A	35	44 ± 4	1.93	40	12.5	3.8
	KANO	NA	−19.19	19.44	8A	32	41 ± 2	1.84	40	7.5	3.7
	OKAM	NA	−20.41	18.22	8A	21	41 ± 1	1.69	40	2.5	3.6
	WEWE	NA	−21.21	16.81	8A	38	39 ± 1	1.75	40	2.5	3.7
	WIN	NA	−22.57	17.10	AF	31	45 ± 5	1.74	42	7.5	3.8
	Ave.						**43**		**41**	**5.7**	**3.7**
E.Tokwe Block	ESPU	MZ	−20.46	32.77	6H	6	39 ± 1	1.76	40	10	3.9
	Ave.						**39**		**40**	**10**	**3.9**
Kheis Province	PKA	SA	−29.67	22.76	AF	10	38 ± 4	1.72	38	7.5	3.8
	Ave.						**38**		**38**	**7.5**	**3.8**
Limpopo Belt	SIRH	SA	−22.95	31.22	6H	6	47 ± 3	1.72	38	12.5	3.9
	PNDA	SA	−22.69	31.01	6H	5	41 ± 1	1.82	43	12.5	3.8
	MSNA	SA	−22.35	30.02	AF	17	47 ± 2	1.72	46	7.5	3.8
	Ave.						**42**		**43**	**10.8**	**3.8**
Mozambique Belt	INCA	MZ	−19.22	33.84	6H	4	29 ± 3	1.81	30	5	3.8
	MACO	MZ	−17.96	34.17	6H	31	32 ± 2	1.72	33	7.5	3.9
	MANI	MZ	−18.95	32.88	6H	8	37 ± 2	1.72	35	5	3.8
	NAPU	MZ	−15.08	39.25	XV	25	42 ± 1	1.70	40	12.5	3.7
	PNG	MZ	−19.00	34.23	6H	23	28 ± 1	1.86	30	7.5	3.8
	SUSS	MZ	−19.42	33.29	6H	12	38 ± 2	1.64	38	7.5	3.8
	CAIA	MZ	−17.8	35.42	6H	4	33 ± 1	1.68	33	5	3.7
	Ave.						**34**		**34**	**6.9**	**3.8**
Namaqua-Natal Belt	SOE	SA	−32.71	25.56	AF	9	43 ± 3	1.75	43	2.5	3.7
	Ave.						**43**		**43**	**2.5**	**3.7**
Cape Fold Belt	GRHM	SA	−33.28	26.38	AF	5	39 ± 1	1.66	40	5	3.7
	Ave.						**39**		**40**	**5**	**3.7**
Rehoboth Province	AIAI	NA	−27.92	17.49	8A	3	–	–	35	12.5	3.8
	AROB	NA	−26.80	19.65	8A	10	40 ± 3	1.89	40	2.5	3.7
	ARON	NA	−24.14	19.12	8A	9	48 ± 4	1.71	45	7.5	3.7
	HELM	NA	−25.88	16.83	8A	10	41 ± 1	1.72	40	15	3.8
	KETS	NA	−26.84	17.94	8A	7	39 ± 2	1.69	38	7.5	3.8
	MARI	NA	−24.60	17.93	8A	9	50 ± 3	1.71	48	10	3.8
	SOLI	NA	−23.86	16.04	8A	10	45 ± 6	1.72	40	12.5	3.8
	WAND	NA	−24.65	19.74	8A	11	41 ± 2	1.80	40	5	3.6
	Ave.						**43**		**41**	**9.1**	**3.8**
S. Irumide Belt	SENA	MZ	−17.45	35.03	XV	18	31 ± 1	1.78	33	7.5	3.8
	TETE	MZ	−16.13	33.57	XV	12	39 ± 1	1.78	40	12.5	3.8
	Ave.						**35**		**36**	**10**	**3.8**
Saharan Metacraton	AMDT	UG	1.95	34.94	XW	33	38 ± 1	1.73	38	5	3.8
	KABG	UG	3.51	34.14	XW	11	40 ± 2	1.78	42	7.5	3.7
	KITG	UG	3.29	32.88	XW	30	35 ± 1	1.68	37	5	3.7
	KOTD	UG	3 0.00	34.11	XW	34	37 ± 1	1.69	40	5	3.8
	LANG	UG	2.74	33.56	XW	24	37 ± 1	1.73	36	5	3.7
	NAPK	UG	2.37	34.38	XW	27	37 ± 2	1.69	37	2.5	3.7
	Ave.						**38**		**38**	**5**	**3.7**
N. Uganda Terrane	GULU	UG	2.88	32.28	XW	32	39 ± 1	1.66	40	2.5	3.7
	KUMI	UG	1.48	33.86	XW	25	40 ± 1	1.75	40	2.5	3.7
	LIRA	UG	2.11	33.06	XW	40	41 ± 5	1.68	40	2.5	3.7
	Ave.						**40**		**40**	**2.5**	**3.7**
Witwatersrand Terrane	BERG	SA	−25.43	31.45	6H	8	37 ± 2	1.66	36	5	3.7
	SNKL	SA	−28.28	27.77	AF	24	37 ± 2	1.79	38	5	3.7
	WDLM	SA	−26.42	27.42	AF	36	40 ± 1	1.68	40	5	3.8
	ORPN	SA	−24.48	31.39	6H	6	33 ± 1	1.70	33	2.5	3.7
	Ave.						**37**		**37**	**4.4**	**3.7**

MLC, mafic lower crustal layer thickness; KC, Kaapvaal Craton.
Countries: MZ, Mozambique; NA, Namibia; SA, South Africa; UG, Uganda.
Depth (1) - Crustal thickness obtained from using the H-κ stacking method, assuming a crustal V_P of 6.5 km/s.
Depth (2) - Crustal thickness obtained from using the Joint Inversion method.

folded metasedimentary sequence locally intruded by small granitoid bodies at ca. 1.7–1.6 Ga and voluminous granitoid batholiths at ca. 1.0–0.9 Ga (Daly and Unrug, 1982; Johnson et al., 2005, 2007). To the southeast and south lie the Southern Irumide and Zambezi Belts, respectively. The Mesoproterozoic Southern Irumide Belt consists of a stack of arc-related terranes associated with the Irumide Orogeny (~1.3–1.0 Ga). The Neoproterozoic Zambezi Belt (880–820 Ma) is made up of marginal zones of remobilized, partially mylonitized Archean and Paleoproterozoic basement rock overlain by a Neoproterozoic sequence of psammites, pelites, carbonate and calc-silicate rocks, as well as minor metavolcanics (Hanson et al., 1988, 1994; Katongo et al., 2004). To the southwest of the Bangweulu Block is the Lufilian Arc (560–550 Ma), which consists of Neoproterozoic volcanics and sediments lying on top of deformed basement rocks (Porada and Berhorst, 2000).

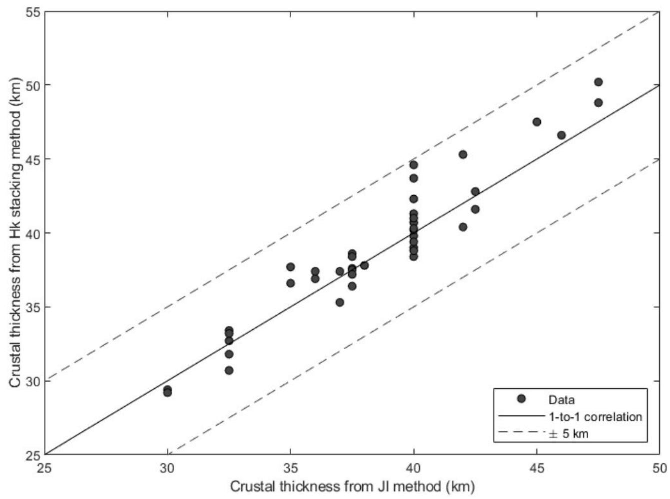

Fig. 6. Plot showing a comparison of crustal thicknesses obtained from the H-k stacking method and the joint inversion (JI) method. The solid line shows a 1-to-1 correlation, and the dashed grey lines show ±5 km from the 1-to-1correlation line.

East of the Tanzania Craton is the Neoproterozoic Mozambique Belt. It consists of reworked Archean crust and younger Pan-African granulite-facies metamorphosed rocks of plutonic origin, uncomformably overlain by ca. 800–550 Ma low-grade metasedimentary rocks (Muhongo and Lenoir, 1994; Pinna et al., 1993). To the north of the Tanzania Craton and on the western and eastern sides of the Paleoproterozoic Aswa Shear Zone lie the Neoarchean Northern Uganda Terrane and the Paleoproterozoic Saharan Metacraton (sometimes referred to as the Nile Craton), respectively (Abdelsalam et al., 2002).

3.3. Central Africa

The Congo Craton forms the nucleus of the Precambrian geological framework of central Africa. The craton is made up of Mesoarchean terranes welded together by Paleo- and Mesoproterozoic belts. The southeastern portion is comprised of the Kasai Block, a 3.1–2.9 Ga Neoarchean granitic-gneissic complex, which underwent granulite-facies metamorphism at ca. 2.8 Ga and 2.4 Ga, overlain by a low-grade volcano-sedimentary unit and cut by granite plutons (ca. 2.1 Ga) (Batumike et al., 2009; Delhal et al., 1986; Walraven and Rumvegeri, 1993). The Neoarchean Angolan Block, in the southwestern region of the craton, is largely comprised of gneisses, metasediments, a 2.8 Ga gabbro-charnockite complex, and 2.6 Ga granitic intrusions (Trompette, 1994). The northwest corner of the craton is comprised of the Ntem

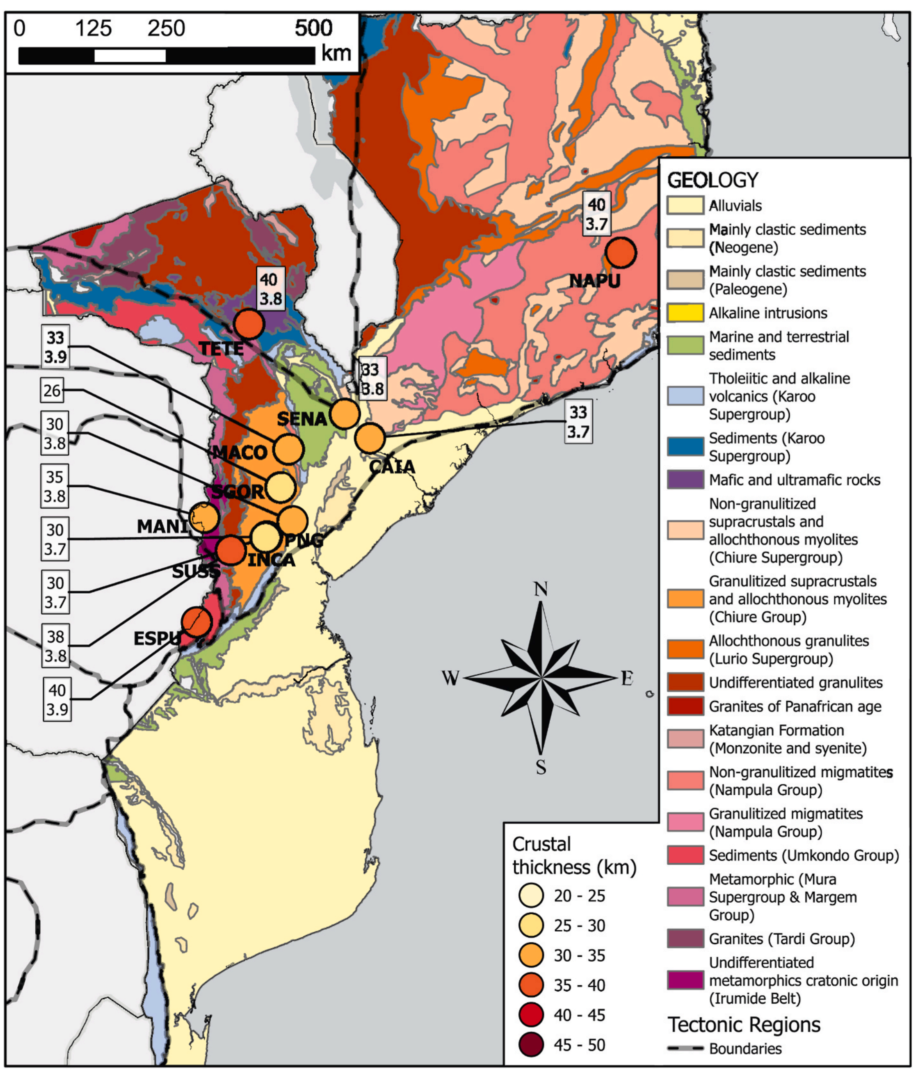

Fig. 7. Geology map of Mozambique showing crustal thicknesses (km) and average crustal Vs (km/s) for each seismic station (coloured circles) (map modified from Schluter, 2008). Bold grey lines show the Precambrian terrane boundaries from Fig. 1.

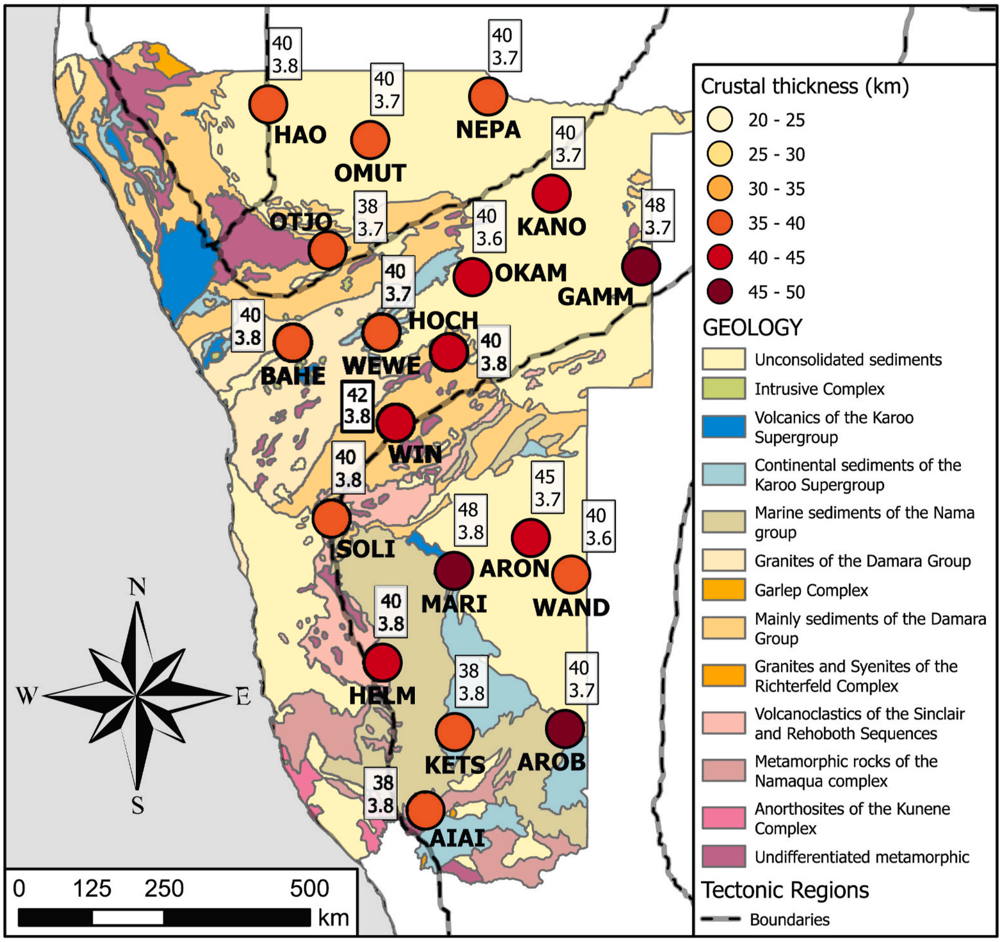

Fig. 8. Geology map of Namibia showing crustal thicknesses (km) and average crustal Vs (km/s) for seismic stations (coloured circles) (map modified from Schluter, 2008). Bold grey lines show the Precambrian terrane boundaries from Fig. 1.

Complex, consisting of 3.2–3.0 Ga migmatites, gneisses and 2.9–2.5 Ga granites cutting into greenstone belt remnants (Shang et al., 2004; Tchameni et al., 2001; Toteu et al., 1994). Along the western margin of the Congo Craton is the West Central African Belt (2.5–2.0 Ga), which also contains early Neoproterozoic rift-related sequences associated with the breakup of Rodinia resting uncomformably on Archean rocks, which were metamorphosed and intruded by 2.1–1.9 Ga granitoids (Feybesse et al., 1998; Penaye et al., 2004). The Bomu-Kibalian Shield located in the northeastern part of the craton contains 3.4 Ga gneisses, 3.0–2.6 Ga greenstone belts, and 2.5–2.6 Ga metamorphosed granites (Cahen et al., 1984; Goodwin, 1990; Lavreau and Deblond, 2000).

3.4. Western Africa

The West African Craton consists of three domains, but only one of them, the Leo (Guinea) Rise falls within the study area (Fig. 1). The Leo Rise can be divided into a western Archean portion, the Man Shield (2.7 Ga), and an eastern Birimian portion known as the Baoulé-Mossi domain (Abouchami et al., 1990; Boher et al., 1992). The former is made up of 3.5 Ga migmatitic orthogneisses and 3.3–3.1 Ga greenstone belts, while the latter contains 2.2–2.1 Ga volcanics and sediments, which were folded and intruded by granites during the Eburnian Orogeny (Hirdes and Davis, 2002; Parra-Avila et al., 2017). Further east lies the Benin-Nigeria Shield, which is a microcontinental block containing 3.7–2.9 Ga gneisses and deformed Birimian greenstone belts intruded by 2.1–1.7 Ga granites, as well as Pan-African granites. Between 640 and 615 Ma, it docked with the passive margin of the West African Craton, creating the Neoproterozoic Dahomeyan Belt, bringing about the closure of the Pharusian Ocean (Affaton et al., 1991; Wright et al., 1985). South of the Benin-Nigerian Shield is the Oubanguides Belt (Central African Fold Belt), which forms a wide corridor between north and central Africa. It contains late Neoproterozoic charnockites and metasediments, accompanied by granitoid plutonism at 565 Ma (Toteu et al., 2001, 2004).

4. Data and methods

4.1. Data

Estimates of crustal structure used in this study come from seismic data collected by many networks over several decades (Fig. 1). Data acquired specifically as part of the AfricaArray initiative come from the AF, 8A, XW, ZP, XJ, YQ, NJ, GH, XV networks (Fig. 1). Data used to obtain the 48 new estimates of crustal structure reported in this study come from 19 stations in the AfricaArray – Namibia network (8A network code) (Nyblade, 2015), six stations in the AfricaArray network in South Africa (AF network code) (Penn State University, 2004), nine stations in the AfricaArray - NE Uganda network (XW network code) (Nyblade, 2017), eight stations in the Mozambique Rift Tomography network (MOZART; 6H network code) (Helffrich and Fonseca, 2011) and three stations in the Investigation of sources of Intraplate Volcanism using PASSCAL Broadband Instruments in Madagascar, The Comoros, and Mozambique network (MACOMO; XV network code) (Wysession et al., 2015).

For the joint inversion method, Rayleigh wave group velocities for periods ranging from 15 to 80 s were obtained for all stations from

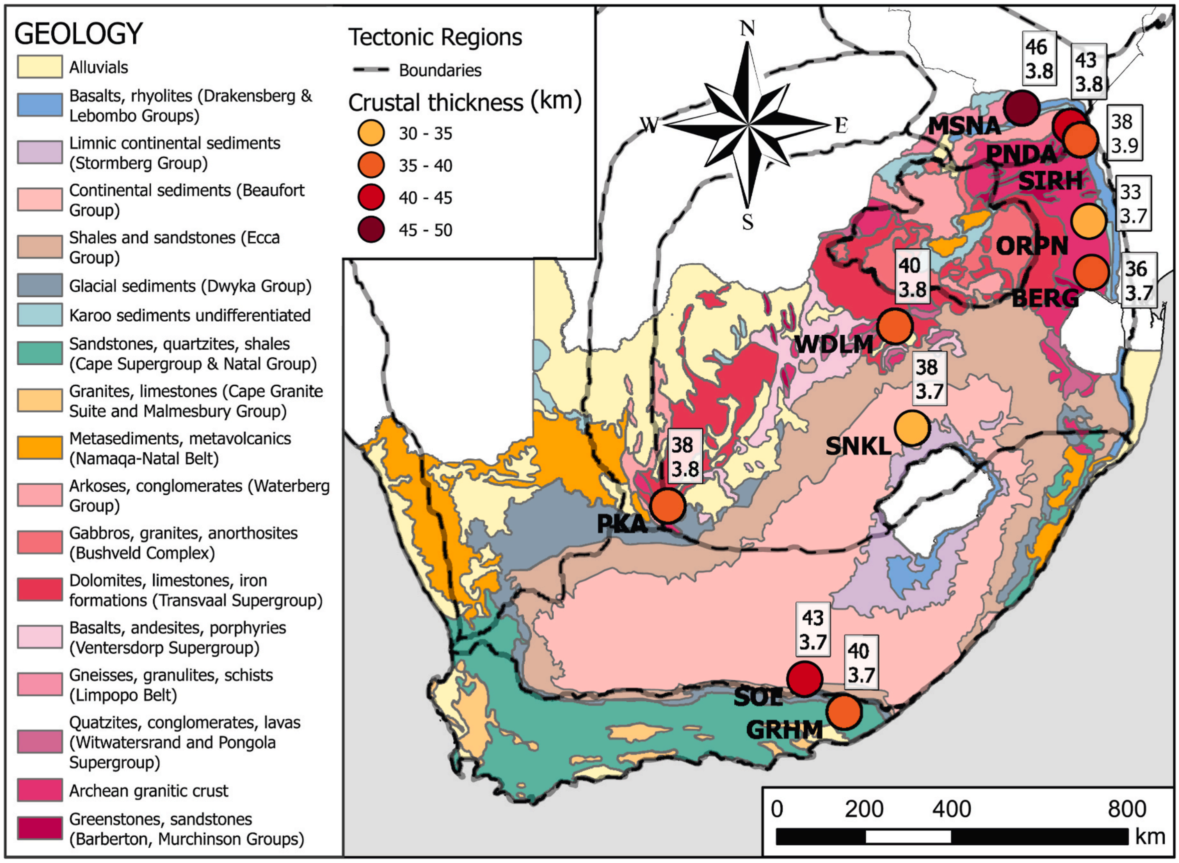

Fig. 9. Geology map of Namibia showing crustal thicknesses (km) and average crustal Vs (km/s) for seismic stations (coloured circles) (map modified from Schluter, 2008). Bold grey lines show the Precambrian terrane boundaries from Fig. 1.

Raveloson et al. (2015). In addition, for stations in South Africa and Mozambique, Rayleigh wave group velocities for periods between 5 and 35s were used from an ambient noise tomography by Fadel et al. (unpublished). To merge group velocities from the two studies to create a composite group velocity curve, group velocities in the 15–35 s period range were averaged. The dispersion curves for all stations were then smoothed using a three-point running average applied over the entire range of periods.

4.2. P-wave receiver functions

Receiver functions are time series computed from three-component seismic data that reveal the impulse response of Earth structure beneath a seismometer (Langston, 1979). The main phases commonly observed in P-wave receiver functions include the direct P wave, the P-to-S conversion (Ps) at the crust-mantle boundary (Moho), and the reverberations between the Moho and free surface (PpPs and PsPs + PpSs; Fig. 2). The arrival times and amplitudes of these phases allow constraints to be placed on the subsurface structure beneath a recording station and can hence be used to estimate crustal thicknesses and velocities, including the crustal P-wave/S-wave velocity ratio (Vp/Vs) (Zhu and Kanamori, 2000).

P-wave receiver functions were computed for each station using waveforms from seismic events with magnitudes equal to 5.5 or greater recorded at epicentral distances ranging from 30° to 90° (Fig. 3). The mean and trend were removed from the original seismograms, which were then tapered and bandpass filtered from 0.05 Hz to 8 Hz, as well as cut to 10 s before and 110 s after the P-wave arrival. To obtain the transverse and radial components of the seismograms, the horizontal components were rotated to the great circle path. The iterative time-domain deconvolution method (Ligorria and Ammon, 1999) was then applied to deconvolve the vertical component from the radial and tangential components. This was done using Gaussian width factors of 1.0 ($f \leq 0.5$ Hz) and 2.5 ($f \leq 1.25$ Hz).

Quality control was carried out on the receiver functions using a least squares minimization of the difference between the original and predicted radial components. The latter was generated through the convolution of the original vertical component and the radial receiver function. Receiver functions showing an 85 % or greater similarity were selected for further analysis.

4.3. H-κ stacking method

The H-κ stacking method of Zhu and Kanamori (2000) was used to estimate Moho depth (H) and average crustal Vp/Vs ratio (κ). The method uses phase arrival times and amplitudes from the Moho Ps and from one or more multiples (PpPs and PpSs + PsPs). This method involves converting the receiver functions in the time domain to H-κ parameter space using an objective function:

$$s(H,\kappa) = \sum_{j=1}^{N} w_1 r_j(t_1) + w_2 r_j(t_2) - w_3 r_j(t_3) \qquad \text{(eq. 1)}$$

where t_i are the travel times of the Moho Ps phase and the two multiples (PpPs, and PsPs + PpSs), w_i are the weights for each phase r_j for the *j*th receiver function, and N is the number of receiver functions. Optimal values of H and κ are determined when $s(H, \kappa)$ has reached its maximum for a simple layer over a half space model within a parameter space extending from 20 to 60 km for H and 1.4 to 2.5 for κ. These values are used as estimates for the Moho depth and Vp/Vs ratio, respectively, beneath a station (Zhu and Kanamori, 2000).

Applying the H-κ stacking method to receiver functions requires

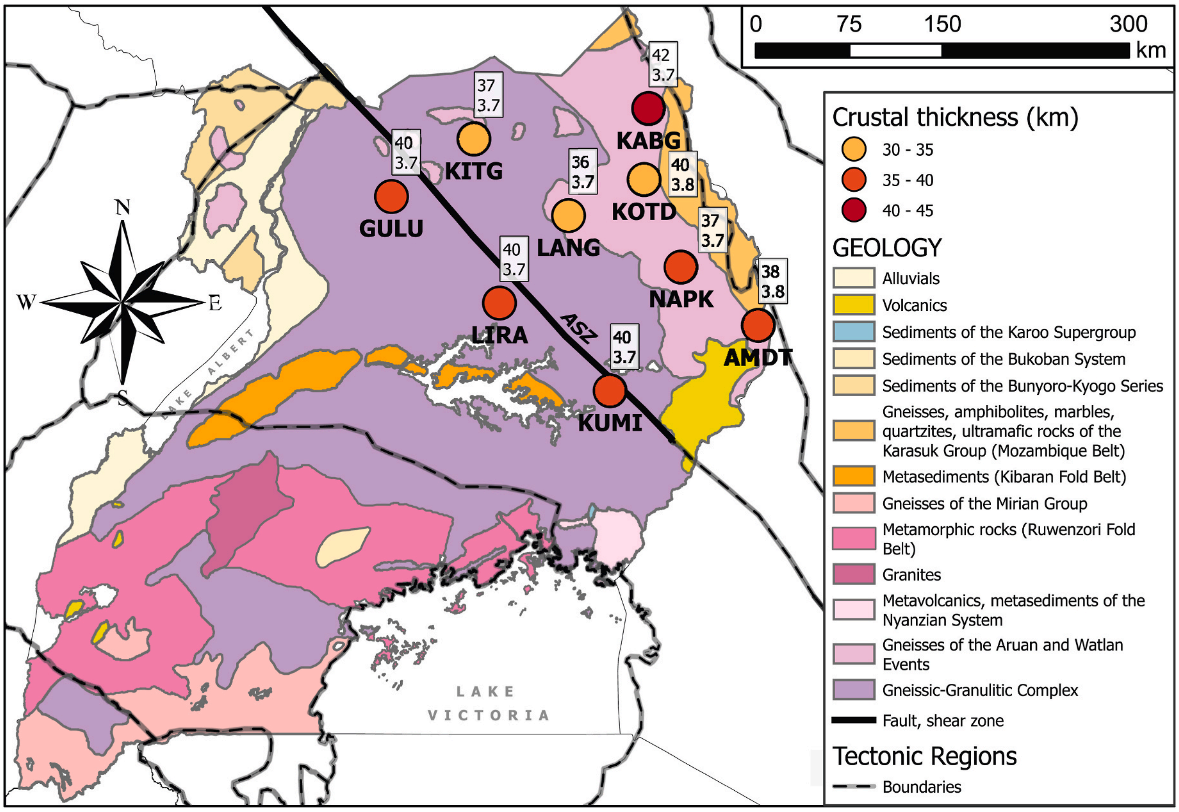

Fig. 10. Geology map of Uganda with crustal thicknesses (km) and average crustal Vs (km/s) displayed for station stations (coloured circles) (map modified from Schluter, 2008). Bold grey lines show the Precambrian terrane boundaries from Fig. 1.

weights for the converted phases be selected and also an average crustal Vp. The three weights should add up to 1.0, with the highest weight being associated with the clearest phase. A weighting system of $w_1 = 0.4$, $w_2 = 0.3$ and $w_3 = 0.3$ was utilized to assign close to similar importance to each of the three phases. A Vp of 6.5 km/s was used as it represents a reasonable average P-wave velocity for Precambrian crust (Christensen and Mooney, 1995) and is consistent with average crustal P-wave velocities reported in many previous studies in eastern and southern Africa (e.g., Fuchs et al., 1997; Julia et al., 2005; Tugume et al., 2013; Kachingwe et al., 2015).

Formal uncertainties for H and κ were estimated from the bootstrapping method, which repeats the summation procedure 200 times with random resampled data (Efron and Tibshirani, 1991). In addition, uncertainty in H and κ arise from the mean crustal Vp used for the computation. P-wave velocities of 6.3 and 6.7 km/s were therefore utilized to place lower and upper bounds on crustal thickness estimates and Vp/Vs ratios. Overall, the uncertainty in crustal thickness associated with the H-κ stacking method was found to be ~3–5 km and ~0.1 for Vp/Vs. Fig. 4 illustrates the H-κ stacking results with formal uncertainties for one station with the H and κ scales zoomed to a narrow range so the 95 % confidence bound can be clearly seen.

4.4. Joint inversion of receiver functions

1-D shear wave velocity models were generated for each station using a joint inversion of P-wave receiver functions and Rayleigh wave group velocities. The joint inversion method used is a linearized, damped least squares method developed by Julia et al. (2000) and involves combining receiver functions, which constrain shear wave velocity contrasts at interfaces, and Rayleigh wave group velocity curves, which constrain average Vs at depth.

Prior to performing the inversion, receiver functions were binned and stacked by similar ray parameter in groups for up to two sets of overlapping frequency bands corresponding to Gaussian width factors of 1.0 and 2.5. This helped to resolve gradual versus sudden velocity changes (i.e., discontinuities) in the 1-D models obtained from the inversion (Julia et al., 2000).

The starting model used in the joint inversion is a 38 km thick crust lying over a Preliminary Reference Earth Model (PREM) (Dziewonski and Anderson, 1981) mantle. The starting model is the same one used in Tugume et al. (2013) and is representative of average crustal structure in eastern and southern Africa. Poisson's ratio in the crust was set to 0.26 ($\kappa = 1.75$) and the model was parametrized with constant velocity layers that increase with depth. Layer thicknesses were set to 1 km in the first 10 km of the model and 2.5 km below 10 km depth. The density for the starting model was determined using the empirical Vs –density relation in Brocher (2005), no model smoothing was applied, and an influence factor to 0.5 was used in the inversions to give equal weight to the receiver function stacks and dispersion measurements. Fig. 5 illustrates the data and results from the joint inversion method for one station.

To estimate the uncertainties of the velocity models, the approach developed by Julia et al. (2000) was followed, which involves repeatedly performing the inversions using a range of inversion parameters, and then examining the models to see how much Vs in any layer changes or by how much the depths of velocity discontinuities change. By repeatedly performing the inversions with a range of inversion parameters to estimate uncertainty, the limitation of not having a normally distributed set of observations, which is required by many methods used to formally estimate uncertainty, is addressed (Julia et al., 2000). Repeatedly performing the inversions using a range of inversion parameters (data weighting, smoothing and starting model; see below), yields an uncertainty of approximately 0.1–0.2 km/s for the velocity in each layer, which translates into an uncertainty of ~2–3 km in the depth of the Moho or any other velocity boundary in a model. For the starting model, we used three constant-velocity models with shear wave velocities of 3.5, 3.9, and 4.3 km/s and the same layer thicknesses described

Table 2
Summary of crustal structure for tectonic provinces (terranes).

Age	Tectonic Province	n[a]	Ave. Depth (km) ± SD	Ave. MLC[b] (km) ± SD	Ave. Vs (km/s) ± SD	Source(s)[c]
Mesoarchean	Swaziland Terrane	3	37 ± 3.1	11 ± 1.2	3.7 ± 0.1	11
	Witwatersrand Terrane	19	38 ± 2.8	5.1 ± 3.8	3.7 ± 0.1	1, 11, 20
	E.Tokwe Block	4	37 ± 1.8	8.1 ± 3.7	3.7 ± 0.1	6, 11
	Kimberley Terrane	28	37 ± 2.4	2.7 ± 1.9	3.7 ± 0.1	6, 11
	Pietersburg Terrane	4	39 ± 2.7	6.7 ± 3.1	3.7 ± 0.1	6, 11
	Average		38 ± 3	6.8 ± 3	3.7 ± 0.1	
Neoarchean	Dodoman Block	8	39 ± 1.8	4.0 ± 3.7	3.8 ± 0.1	6, 11
	Angolan Block	5	39 ± 1.3	6.1 ± 4.5	3.7 ± 0.1	1, 10
	Nyanzian Block	29	37 ± 2.6	3.3 ± 2.5	3.7 ± 0.1	9, 10, 13, 17
	W.Tokwe Block	6	39 ± 4.8	0.8 ± 1.2	3.7 ± 0.1	4, 6, 11
	Limpopo Belt	16	43 ± 3.2	10 ± 3.8	3.7 ± 0.1	1, 11, 20
	N.Uganda Terrane	17	38 ± 4.0	5.1 ± 4.0	3.7 ± 0.1	1, 3, 5, 17
	Ntem Complex	5	43 ± 2.7	23 ± 3.0	3.9 ± 0.1	1, 10
	Kasai Block	2	36 ± 2.5	4.0 ± 1.0	3.6 ± 0.1	10
	Average		39 ± 4	7.0 ± 5	3.7 ± 0.1	
Paleoproterozoic	Bangweleu Belt	7	41 ± 3.3	2.8 ± 3.3	3.6 ± 0.2	8, 10, 17
	Saharan Metacraton	8	38 ± 1.8	4.3 ± 2.2	3.7 ± 0.1	6, 11
	W. Central African Belt	1	34 ± 0	8.0 ± 0	3.7 ± 0.1	10
	Baoul'e-Mossi Domain	3	43 ± 1.7	16 ± 1.0	3.9 ± 0.1	2, 14
	Benin-Nigerian Shield	3	36 ± 2.9	3.7 ± 0.9	3.7 ± 0.1	2
	Bushveld Complex	9	42 ± 3.1	10 ± 5.0	3.7 ± 0.1	11
	Ubendian Belt	23	40 ± 4.5	4.1 ± 5.3	3.7 ± 0.1	3, 8, 9. 16, 17
	Okwa Terrane	10	42 ± 2.8	7.8 ± 3.8	3.7 ± 0.1	6, 11, 21
	Kheis Province	5	40 ± 2.5	7.5 ± 1.8	3.7 ± 0.1	1, 11, 20
	Usagaran Belt	7	37 ± 1.1	2.7 ± 2.1	3.8 ± 0.1	5, 9, 13, 17
	Rehoboth Province	22	40 ± 3.4	9.4 ± 4.1	3.7 ± 0.1	1, 6, 11, 2
	Average		40 ± 4	6.9 ± 4	3.7 ± 0.1	
Mesoproterozoic	Rwenzori Belt	13	37 ± 1.8	2.3 ± 1.5	3.7 ± 0.1	7, 17, 18
	Kibaran Belt	10	41 ± 1.2	2.6 ± 2.3	3.8 ± 0.1	9, 10, 12, 17
	Irumide Belt	31	41 ± 4.0	5.4 ± 3.9	3.7 ± 0.1	3, 10, 15, 16, 17
	S. Irumide Belt	10	41 ± 3.8	5.2 ± 4.4	3.7 ± 0.1	1, 9, 10, 15, 17
	Namaqua-Natal Belt	11	39 ± 7.5	8.7 ± 5.8	3.7 ± 0.1	1, 11, 20
	Average		40 ± 4	4.8 ± 4	3.7 ± 0.1	
Neoproterozoic	Zambezi Belt	2	36 ± 2.1	3.5 ± 2.1	3.7 ± 0.1	10
	Damara Belt	19	42 ± 3.3	3.9 ± 3.9	3.7 ± 0.1	1, 6, 8, 21
	Dahomeyan Terrane	4	43 ± 1.3	14 ± 2.1	3.8 ± 0.1	2
	Oubanguides	15	36 ± 4.1	4.4 ± 3.5	3.7 ± 0.1	16
	Mozambique Belt	45	38 ± 3.9	4.4 ± 3.2	3.7 ± 0.1	1, 3, 5, 9, 10, 17
	Lufilian Arc	3	37 ± 3.6	4.5 ± 2.5	3.7 ± 0.1	10
	Average		39 ± 4	6.0 ± 5	3.7 ± 0.1	
Overall Average			39 ± 4	6 ± 5	3.7 ± 0.1	

n[a] = Number of stations; **MLC**[b] = Mafic lower crustal layer thickness.
[c]*Sources*: 1 = This study, 2 = Akpan et al. (2016), 3 = Borrego et al. (2018), 4 = Delph and Porter (2015), 5 = Dugda et al. (2005), 6 = Fadel et al. (2018), 7 = Gummert et al. (2016), 8 = Hodgson et al. (2017), 9 = Julia et al. (2005), 10 = Kachingwe et al. (2015), 11 = Kgaswane et al. (2009), 12 = Last et al. (1997), 13 = Plasman et al. (2017), 14 = Sandvol et al. (1998), 15 = Sun et al. (2021), 16 = Tokam et al. (2010), 17 = Tugume et al. (2013), Wölbern et al., (2010); Young, (2012), 18 = Wolbern et al. (2010), 19 = Young (2012), 20 = Youssof et al. (2013), 21 = Yu et al. (2015).

above. We also used three halfspace models with a constant velocity for the crust of 3.9 km/s and a constant velocity for the mantle of 4.5 km/s. We placed the Moho depth in the halfspace models at depths of 36, 40, and 44 km. For data weighting, the inversion procedure was performed by varying the weighting of the receiver functions and dispersion curves in 10 % increments (i.e., 30 %/70 %, 40 %/60 %, 50 %/50 %, 60 %/40 %, and 70 %/30 %). And for smoothing, we performed inversions with smoothing values of 0.1, 0.3, 0.6, and 0.9.

5. Results

In this section, crustal thicknesses, average S wave velocities, and the average thickness of mafic layers within the crust are reviewed. Results are summarized in Table 1. The H-κ stacking and joint inversion results for all stations are provided in the supplemental material.

1-D Vs models obtained from the joint inversion of receiver functions and group velocities can be used to identify the Moho and the thickness of mafic layering in the crust. Given that velocities greater than 4.3 km/s are considered typical for mantle material (Christensen and Mooney, 1995), the depth at which Vs exceeded 4.3 km/s was used to determine Moho depth on the 1-D models. In many of the models, the depth at which Vs reaches or exceeds 4.3 km/s is also coincident with a velocity discontinuity (jump). The thickness of mafic lower crust was determined using model layers where Vs is between 4.0 and 4.3 km/s (Christensen and Mooney, 1995).

Within the reported uncertainties, a 1-to-1 correlation is found between the estimates of crustal thickness determined using the joint inversion and H-κ stacking methods for the 48 stations with new results reported in this study (Fig. 6), illustrating consistent results between the two methods.

5.1. Mozambique

Stations in Mozambique are mainly located in the Mozambique Belt, with a few located in the East Tokwe (station ESPU) and Southern Irumide (stations SENA and TETE) terranes. Crustal thicknesses range from 30 to 40 km (Fig. 7; Table 1), and the average shear wave velocities are between 3.7 and 3.9 km/s. Seven to 10 km of mafic lower crust is present beneath many of the stations (Table 1).

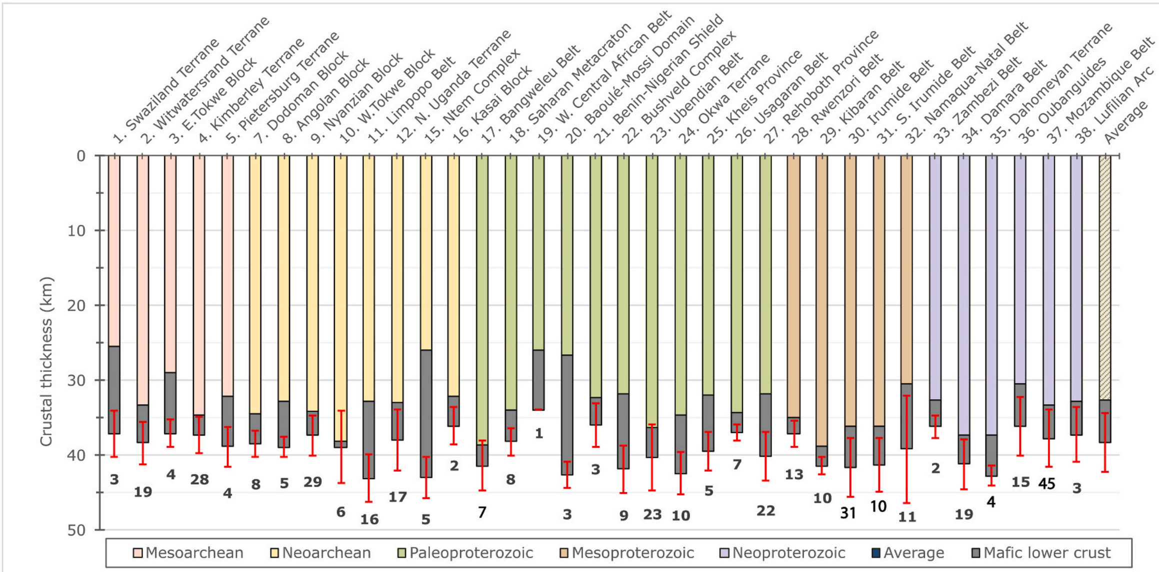

Fig. 11. Summary of average crustal thicknesses (km) associated with each tectonic province (terrane). Terranes are numbered to match the order in the map key (Fig. 1) and coloured by age. Mafic lower crustal layers are shown in dark grey, and the number of stations used in the compilation is displayed above each bar. Dashed lines show the average crustal thickness range (i.e., 39 ± 4 km), and the red error bars show ± 1 standard deviation of the average crustal thickness for each terrane.

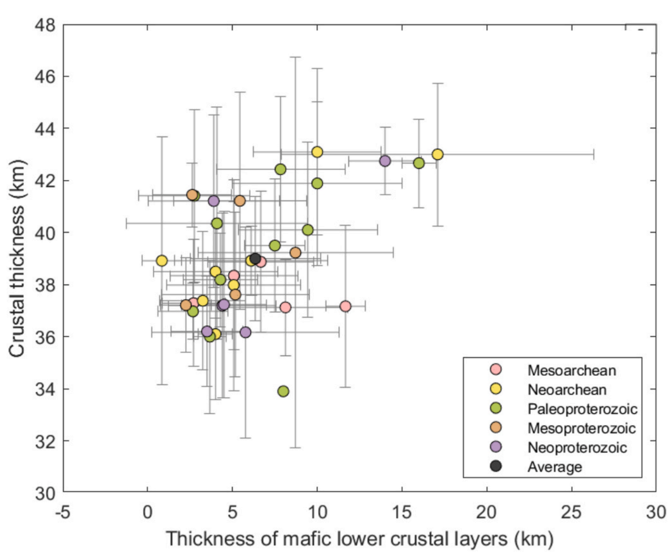

Fig. 12. Plot showing the thickness of the crust associated with each terrane as a function of the thickness of lower crustal layers with a shear wave velocity 4.0–4.3 km/s (i.e., mafic lower crust). Data are grouped by terrane age.

5.2. Namibia

The crustal thickness beneath stations in Namibia ranges from 35 to 48 km (Table 1; Fig. 8). The Neoarchean Angolan Block, which extends into northern Namibia, has an average crustal thickness of 39 km. The mafic lower crust is about 2.5 km thick on average. The Paleoproterozoic Rehoboth Province has slightly thicker crust, with an average thickness of about 41 km, and the Neoproterozoic Damara Belt also has an average crustal thickness of 41 km. The Rehoboth Province and the Damara Belt have on average 5 and 9 km of mafic lower crust, respectively. Average shear wave velocities are consistent across the aforementioned terranes, between 3.7 and 3.8 km/s.

5.3. South Africa

For stations located in the Witwatersrand terrane (Fig. 9), the average crustal thickness ranges from 33 km to 40 km, with an overall average of 37 km (Table 1). Evidence for mafic layering in the lower crust of 2.5–5 km is found. Station PKA is located in the southern part of the Kheis Province that borders the Kimberley terrane. It has a 38-km thick crust and shows evidence for the presence of an 8-km thick mafic lower crustal layer. Further south, station SOE in the southern Mesoproterozoic Namaqua-Natal Fold Belt has a crustal thickness of 43 km and a 2.5-km-thick mafic lower crustal layer. And station GRHM in the Cape Fold Belt (or Saldania) has a 40-km-thick crust and a 9-km thick mafic lower crust. Finally, two stations (MSNA, PNDA) in the Neoarchean Limpopo Belt have crustal thicknesses of 43–46 km, as well as a mafic lower crust thickness of 11 km. Average crustal shear wave velocities for stations in South Africa range between 3.7 and 3.8 km/s.

5.4. Uganda

Results obtained from the Northern Uganda Terrane and Saharan Metacraton in Uganda show average crustal thicknesses for 40 km and 38–42 km, respectively (Table 1, Fig. 10), and are consistent with results reported by Ogden et al. (2023) and Wang et al. (2022). The overall average crustal thickness is 40 km for the former terrane and 38 km for the latter terrane. The mafic lower crust in the Northern Uganda Terrane and Saharan Metacraton averages 2 and 5 km, respectively. The average shear wave velocity obtained from both tectonic terranes is about 3.7 km/s.

6. Discussion

We combine the new estimates of crustal thickness and shear-wave velocities with published results and examine the data compilation for secular trends in crustal thickness and/or composition, as reflected in Moho depths, the thickness of the mafic lower crust, and average crustal Vs. Shown in Table 2 and illustrated in Fig. 11 are average Moho depths, crustal Vs, and thickness of the mafic lower crust for each terrane in Fig. 1, obtained by combining our new results with results in previously published studies (Table S1). Results from seismic stations located in

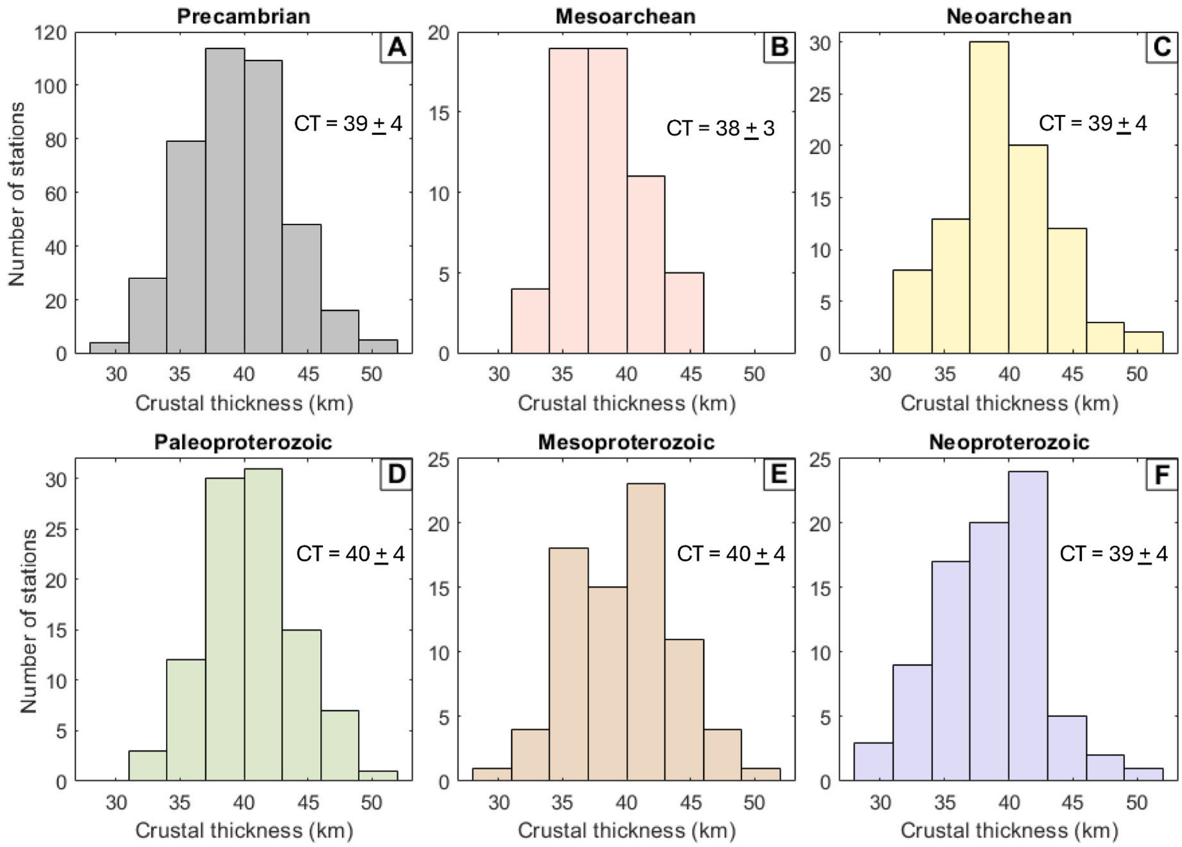

Fig. 13. Plots showing the distribution of crustal thickness (CT; km) results for stations located on terranes of Precambrian (All) (A); Mesoarchean (B); Neoarchean (C); Paleoproterozoic (D); Mesoproterozoic (E); and Neoproterozoic (F) age. Average crustal thickness ±standard deviation results are shown for each time period.

areas affected by Phanerozoic tectonism (i.e., Karoo and East African rifts) are not included in the data compilation.

The average crustal thicknesses for Archean and Proterozoic terranes are essentially the same, 39 ± 2 (1 s.d.) km and 39 ± 3 km, respectively, and the average crustal thickness of all Precambrian terranes is 39 ± 4 km (Table 2). These averages are consistent with results published by Kachingwe et al. (2015) using a smaller dataset. While crustal thickness beneath most stations falls within one standard deviation of the average thickness (i.e., 39 km), the West Central African Belt (34 km), for which there is only one data point, is a notable exception. The Limpopo Belt (43 km), the Ntem Complex (43 km), the Dahomeyan Terrane (43 km), and the Baoulé-Mossi Domain (43 km) may have somewhat thicker than average crust, although results fall within the one standard deviation of the average (Table 2). The greater crustal thickness of the Limpopo Belt, compared to the average (39 km), was noted previously. For example, studies by de Wit et al. (1992), Nguuri et al. (2001), and Treloar et al. (1992) found similarly thick crust beneath the Limpopo Belt, which they attributed, in part, to crustal thickening associated with the Limpopo Orogeny (~2.7–2.6 Ga).

Results for the Baoulé-Mossi domain in West Africa are also consistent with previous research suggesting that the terrane is associated with crustal shortening and thickening, as it evolved in a compressional-type environment. According to Parra-Avila et al. (2017, 2019), the domain developed in an arc setting between ca. 2.25–2.1 Ga, which later transformed into a collision-type setting after ca. 2.1 Ga. The Dahomeyan terrane, which spans 1000 km and connects the Baoulé-Mossi domain with the Benin-Nigerian Shield, also shows evidence of crustal thickening. These findings can be explained by previous petrological, geochemical, and geochronological studies focused on the ultramafic and mafic massifs of the Dahomeyan terrane, highlighting the latter's geodynamical evolution and relevance to the closure of the Pharusian ocean during the Neoproterozoic (e.g., Berger et al., 2011; Caby et al., 2008; Ganade de Araujo et al., 2014; Guillot et al., 2019). Those studies suggest the massifs are associated with a Neoproterozoic intra-oceanic arc that formed near or at the western margin of the Benin-Nigerian Shield and were incorporated into the lower plate during the continental subduction of the West African Craton, which occurred c. 620-610 Ma.

Finally, the Ntem Complex, located in southern Cameroon, is also associated with thicker than average crust. This has been well documented by previous studies and is believed to be a relict feature from a continent-continent collision during the formation of Gondwana, which caused overthrusting of Pan-African units onto the craton (Penaye et al., 1993; Tadjou et al., 2009; Toteu et al., 2004). This collision occurred along the northern boundary of the Congo Craton and led to the formation of a suture zone between the Congo Craton and the Oubanguides Belt (Tadjou et al., 2009; Tokam et al., 2010; Gallacher and Bastow, 2012).

For all terranes, the average crustal shear wave velocities are between 3.6 and 3.9 km/s, with an average of 3.7 ± 0.1 km/s (Table 2). All average terrane velocities fall within one standard deviation of the mean velocity. All Precambrian terranes have high shear wave velocity layers (V_s = 4.0–4.3 km/s) in the lowermost crust, which we have attributed to mafic lithologies (e.g. Christensen and Mooney, 1995; Rudnick and Fountain, 1995; Rudnick and Gao, 2003). The thickness of the mafic lower crust varies between 1 and 23 km. The Ntem Complex has an anomalously thick mafic lower crust, more than twice as thick as beneath any other Archean terrane. For Archean terranes, the average thickness of the mafic lower crust is 7 ± 4 km, and, for Proterozoic terranes, the average is 6 ± 4 km.

Overall, as can be seen in Fig. 11 and Table 2, we do not find evidence for the presence of age-related trends in crustal thickness and mean crustal velocity. Results of crustal thickness and crustal composition, as reflected in the thickness of the mafic lower crust and the average crustal Vs (Table 2, Fig. 12), also show little if any evidence for secular trends. In fact, inter-era variability tends to equal or exceed inter-eon variability. In other words, variability across the Precambrian is not any greater than variability observed over smaller timescales. Thus, our findings are consistent with those published by Rudnick & Fountain (1995), Zandt & Ammon (1995), Tugume et al. (2012, 2013), Stankiewicz & de Wit (2013), and Kachingwe et al. (2015), which argue for no significant variability in mean crustal thickness, crustal velocity or inferred composition of Archean and Proterozoic crust. This lack of secular variation can be explained by either very little change in the processes involved in crustal genesis over much of Earth's history, or alternatively, by the crust being modified by later tectonic and/or magmatic events to the point where secular trends in crustal genesis have ceased to be observable.

Histograms in Fig. 13 further illustrate the distribution of crustal thickness results across Precambrian terranes of different ages. Mesoarchean terrranes display the least amount of spread, while Mesoproterozoic terranes show the most. Even so, as seen in Figs. 11 and 12, no obvious age-related trends are observed in crustal thickness, mafic lower crustal layer thickness, or average crustal Vs.

7. Summary and conclusions

New estimates of Precambrian crustal structure are reported for 48 seismic stations using the H-κ stacking and joint inversion methods, thus contributing further to our knowledge about the structure and composition of the Precambrian crust in sub-Saharan Africa. New results from Namibia are from the Neoarchean Angolan Block, Paleoproterozoic Rehoboth Province and Neoproterozoic Damara Belt, and when combined with previous results, yield average crustal thicknesses to 39, 41, and 41 km, respectively. In Uganda, results for the Neoarchean Northern Uganda Terrane and Paleoproterozoic Saharan Metacraton yield average crustal thicknesses of 40 and 38 km, respectively. In Mozambique, results obtained from stations in western and northern Mozambique provide new constrains on the crustal structure of the Neoproterozoic Mozambique Belt and Mesoproterozoic South Irumide Belt. Average crustal thickness of 34 km and 36 km, respectively, were obtained for those terranes. In South Africa, the Mesoarchean Witwatersrand terrane has an average Moho depth of 37 km, and the Neoarchean Limpopo Belt has a crustal thickness of 43 km.

These new results, combined with results from previous studies, yield an average crustal thickness for all Precambrian terranes of 39 ± 4 km. We find that the average crustal thicknesses are essentially identical for Archean (39 ± 2 km) and Proterozoic (39 ± 3 km) terranes. The average crustal thicknesses for terranes of all eras in the Precambrian all fall between 38 and 40 km. Furthermore, the average thickness of the mafic lower crust is almost identical in Archean and Proterozoic terranes, 7 ± 4 km and 6 ± 4 km, respectively. Finally, the average crustal velocities for all terranes fall within one standard deviation of the mean velocity of 3.7 km/s. These results are consistent with findings in previous studies highlighting a lack of evidence for secular variation in the crustal structure or composition of Precambrian terranes in sub-Saharan Africa, suggesting that secular trends reflecting crustal genesis, if they existed, have been obscured by tectonic reworking of crustal structure and composition by orogenic and/or magmatic events.

CRediT authorship contribution statement

Alexandra Sabattier: Writing – review & editing, Writing – original draft, Methodology, Investigation, Formal analysis, Data curation. **Andrew Nyblade:** Writing – review & editing, Writing – original draft, Validation, Supervision, Project administration, Methodology, Investigation, Funding acquisition, Conceptualization. **Raymond Durrheim:** Writing – review & editing, Validation, Resources, Project administration, Funding acquisition. **Fenitra Andriampenomanana:** Writing – review & editing, Validation, Data curation. **Andriamiranto Raveloson:** Writing – review & editing, Data curation. **Islam Fadel:** Writing – review & editing, Formal analysis, Data curation. **Mark van der Meijde:** Writing – review & editing, Funding acquisition, Data curation. **Amanda Willet:** Methodology, Formal analysis.

Declaration of competing interest

The authors declare that they have no known competing financial interests or personal relationships that could have appeared to influence the work reported in this paper.

Acknowledgements

This work was supported by National Science Foundation grants 0440032, 0530062, 0824781, 110440032, 1128936, and 1634108. R.J. D. acknowledges support from the DST/NRF South African Research Chair program. We thank two anonymous reviewers for helpful and constructive comments.

Appendix A. Supplementary data

Supplementary data to this article can be found online at https://doi.org/10.1016/j.jafrearsci.2025.105664.

Data availability

Data used in this study are openly available from the EarthScope data management center (https://ds.iris.edu/ds/nodes/dmc/).

References

Abbott, D.H., Mooney, W.D., Van Tongeren, J.A., 2013. The character of the Moho and lower crust within Archean cratons and the tectonic implications. Tectonophysics 609, 690–705.

Abdelsalam, M.G., Liégeois, J.-P., Stern, R.J., 2002. The saharan Metacraton. J. Afr. Earth Sci. 34 (3–4), 119–136.

Abouchami, W., Boher, M., Michard, A., Albarede, F., 1990. A major 2.1 Ga event of mafic magmatism in west Africa: an early stage of crustal accretion. J. Geophys. Res. Solid Earth 95 (B11), 17605–17629.

Affaton, P., Rahaman, M.A., Trompette, R., Sougy, J., 1991. The dahomeyide orogen: tectonothermal evolution and relationships with the volta basin. In: Dallmeyer, R.D., Lécorché, J.P. (Eds.), The West African Orogens and Circum-Atlantic Correlatives. Springer, pp. 107–122.

Akpan, O., Nyblade, A., Okereke, C., Oden, M., Emry, E., Julia, J., 2016. Crustal structure of Nigeria and southern Ghana, West Africa from P-wave receiver functions. Tectonophysics 676, 250–260.

Ammon, C.J., Randall, G.E., Zandt, G., 1990. On the nonuniqueness of receiver function inversions. J. Geophys. Res. Solid Earth 95 (B10), 15303–15318.

Batumike, J.M., Griffin, W.L., O'Reilly, S.Y., Belousova, E.A., Pawlitschek, M., 2009. Crustal evolution in the central Congo-Kasai Craton, Luebo, D.R. Congo: insights from zircon U–Pb ages, Hf-isotope and trace-element data. Precambr. Res. 170 (1), 107–115.

Begg, G.C., Griffin, W.L., Natapov, L.M., O'Reilly, S.Y., Grand, S.P., O'Neill, C.J., Hronsky, J.M.A., Djomani, Y.P., Swain, C.J., Deen, T., Bowden, P., 2009. The lithospheric architecture of Africa: seismic tomography, mantle petrology, and tectonic evolution. Geosphere 5 (1), 23–50.

Berger, J., Caby, R., Liégeois, J.P., Mercier, J.C.C., Demaiffe, D., 2011. Deep inside a Neoprotero- zoic intra-oceanic arc: growth, differentiation and exhumation of the Amalaoulaou complex (Gourma, Mali). Contrib. Mineral. Petrol. 162, 773–796.

Boher, M., Abouchami, W., Michard, A., Albarede, F., Arndt, N.T., 1992. Crustal growth in West Africa at 2.1 Ga. J. Geophys. Res. Solid Earth 97 (B1), 345–369.

Borg, G., Krogh, T., 1999. Isotopic age data of single zircons from the Archaæan Sukumaland Green- stone Belt, Tanzania. J. Afr. Earth Sci. 29 (2), 301–312.

Borg, G., Shackleton, R.M., 1997. The Tanzania and NE-zaire cratons. In: De Wit, M.J., Ashwal, L.D. (Eds.), Greenstone Belts. Oxford University Press, pp. 608–619.

Borrego, D., Nyblade, A.A., Accardo, N.J., Gaherty, J.B., Ebinger, C.J., Shillington, D.J., Chindandali, P.R., Mbogoni, G., Ferdinand, R.W., Mulibo, G., O'Donnell, J., Kachingwe, M., Tepp, G., 2018. Crustal structure surrounding the northern Malawi rift and beneath the rungwe volcanic province, east Africa. Geophys. J. Int. 215 (2), 1410–1426.

Brocher, T.A., 2005. Empirical relations between elastic wavespeeds and density in the earth's crust. Bull. Seismol. Soc. Am. 95 (6), 2081–2092.

Caby, R., Buscail, F., Dembele, D., Diakite, S., Sacko, S., Bal, M., 2008. Neoproterozoic garnet- glaucophanites and eclogites: new insights for subduction metamorphism of

the Gourma fold and thrust belt (eastern Mali). Geological Society of London - Special Publications 297 (1), 203–216.
Cahen, L., Snelling, N.J., Delhal, J., Vail, J.R., Bonhomme, M., Ledent, D., 1984. The Geochronology and Evolution of Africa. Clarendon Press, Oxford.
Christensen, N.I., Mooney, W.D., 1995. Seismic velocity structure and composition of the continental crust: a global view. J. Geophys. Res. Solid Earth 100 (B6), 9761–9788.
Daly, M.C., Unrug, R., 1982. The Muva Supergroup of northern Zambia: a craton to mobile belt sedimentary sequence. Trans. Geol. Soc. S. Afr. 85, 155–165.
De Waele, B., 2005. *The Proterozoic Geological History of the Irumide Belt, Zambia* [PhD]. Curtin University of Technology.
De Waele, B., Johnson, S.P., Pisarevsky, S.A., 2008. Palaeoproterozoic to Neoproterozoic growth and evolution of the eastern Congo Craton: its role in the Rodinia puzzle. Precambr. Res. 160 (1), 127–141.
De Waele, B., Kampunzu, A.B., Mapani, B.S.E., Tembo, F., 2006a. The mesoproterozoic Irumide belt of Zambia. J. Afr. Earth Sci. 46 (1), 36–70.
De Waele, B., Liégeois, J.-P., Nemchin, A.A., Tembo, F., 2006b. Isotopic and geochemical evidence of Proterozoic episodic crustal reworking within the Irumide belt of south-central Africa, the southern metacratonic boundary of an Archaean Bangweulu Craton. Precambr. Res. 148 (3), 225–256.
de Wit, M.J., de Ronde, C.E.J., Tredoux, M., Roering, C., Hart, R.J., Armstrong, R.A., Green, R.W.E., Peberdy, E., Hart, R.A., 1992. Formation of an archaean continent. Nature 357 (6379), 553–563.
Delhal, J., Deutsch, S., Denoiseux, B., 1986. A Sm/1bNd isotopic study of heterogeneous granulites from the Archean Kasai-Lomami gabbro-norite and charnockite complex (Zaire, Africa). Chem. Geol. 57 (1), 235–245.
Delph, J.R., Porter, R.C., 2015. Crustal structure beneath southern Africa: insight into how tectonic events affect the Mohorovici´c discontinuity. Geophys. J. Int. 200 (1), 254–264.
Dirks, P.H.G.M., Blenkinsop, T.G., Jelsma, H.A., 2009. The geological evolution of Africa. In: De Vivo, B., Grasemann, B., Stuwe, K. (Eds.), Geology, vol. IV. Eolss Publishers, Oxford, U.K, pp. 230–251.
Dugda, M.T., Nyblade, A.A., Julia, J., Langston, C.A., Ammon, C.J., Simiyu, S., 2005. Crustal structure in Ethiopia and Kenya from receiver function analysis: implications for rift development in eastern Africa. J. Geophys. Res. Solid Earth 110 (B1). https://doi.org/10.1029/2004JB003065.
Durrheim, R.J., Mooney, W.D., 1994. Evolution of the Precambrian lithosphere: seismological and geochemical constraints. J. Geophys. Res. Solid Earth 99 (B8), 15359–15374.
Durrheim, R.J., Nyblade, A.A., 2022. Insights into the structure and geodynamics of the African continent produced by AfricaArray seismograph networks. 17th SAGA Biennial Conference. Extended Abstract, 2022.
Dziewonski, A.M., Anderson, D.L., 1981. Preliminary reference Earth model. Phys. Earth Planet. Inter. 25 (4), 297–356.
Efron, B., Tibshirani, R., 1991. Statistical data analysis in the computer age. Science 253 (5018), 390–395.
Eglington, B.M., Armstrong, R.A., 2004. The Kaapvaal Craton and adjacent orogens, southern Africa: a geochronological database and overview of the geological development of the craton. S. Afr. J. Geol. 107 (1–2), 13–32.
Fadel, I., van der Meijde, M., Paulssen, H., 2018. Crustal structure and dynamics of Botswana. J. Geophys. Res. Solid Earth 123 (12), 10659–10671.
Feybesse, J.L., Johan, V., Triboulet, C., Guerrot, C., Mayaga-Mikolo, F., Bouchot, V., Eko N'dong, J., 1998. The West Central African belt: a model of 2.5–2.0Ga accretion and two-phase orogenic evolution. Precambr. Res. 87 (3), 161–216.
Fuchs, K., Altherr, B., Muller, B., Prodehl, C., 1997. Structure and dynamic processes in the lithosphere of the Afro-Arabian rift system. Tectonophysics 278, 1–352.
Gallacher, R.J., Bastow, I., 2012. The development of magmatism along the Cameroon Volcanic Line: evidence from teleseismic receiver functions. Tectonics 31, TC3018. https://doi.org/10.1029/2011TC003028.
Ganade de Araujo, C.E., Rubatto, D., Hermann, J., Cordani, U.G., Caby, R., Basei, M.A., 2014. Ediacaran 2,500-km-long synchronous deep continental subduction in the West Gondwana Orogen. Nat. Commun. 5 (1), 5198.
Goodwin, A.M., 1990. Precambrian Geology: the Dynamic Evolution of the Continental Crust. Academic Press, p. 666.
Goodwin, A.M., 1996. Principles of Precambrian Geology. Academic Press, p. 340.
Guillot, S., Agbossoumondé, Y., Bascou, J., Berger, J., Duclaux, G., Hilairet, N., Ménot, R. P., Schwartz, S., 2019. Transition from subduction to collision recorded in the Pan-African arc com- plexes (Mali to Ghana). Precambr. Res. 320, 261–280.
Gummert, M., Lindenfeld, M., Wölbern, I., Rümpker, G., Celestin, K., Batte, A., 2016. Crustal struct ure and high-resolution Moho topography across the Rwenzori region (Albertine rift) from P-receiver functions. Geological Society of London - Special Publications 420 (1), 69–82.
Hanson, R.E., Wilson, T.J., Munyanyiwa, H., 1994. Geologic evolution of the Neoproterozoic Zambezi orogenic belt in Zambia. J. Afr. Earth Sci. 18 (2), 135–150.
Hanson, R.E., Wilson, T.J., Wardlaw, M.S., 1988. Deformed batholiths in the Pan-African Zambezi belt, Zambia: age and implications for regional Proterozoic tectonics. Geology 16 (12), 1134–1137.
Helffrich, G., Fonseca, J.F.B.D., 2011. Data from: Mozambique Rift Tomography. International Federation of Digital Seismograph Networks. https://doi.org/10.7914/SN/6H2011.
Hirdes, W., Davis, D.W., 2002. U–Pb geochronology of Paleoproterozoic rocks in the southern part of the Kedougou-Kéniéba Inlier, Senegal, West Africa: evidence for diachronous accretionary development of the Eburnean Province. Precambr. Res. 118 (1), 83–99.
Hodgson, I., Illsley-Kemp, F., Gallacher, R.J., Keir, D., Ebinger, C.J., Mtelela, K., 2017. Crustal structure at a young continental rift: a receiver function study from the Tanganyika Rift. Tectonics 36 (12), 2806–2822.
Jelsma, H.A., Dirks, P.H.G.M., 2002. Neoarchaean tectonic evolution of the Zimbabwe Craton. Geological Society of London - Special Publications 199 (1), 183–211.
Johnson, S.P., de Waele, B., Tembo, F., Katongo, C., Tani, K., Chang, Q., Iizuka, T., Dunkley, D., 2007. Geochemistry, geochronology and isotopic evolution of the chewore–rufunsa terrane, southern Irumide belt: a mesoproterozoic continental margin arc. J. Petrol. 48 (7), 1411–1441.
Johnson, S.P., Rivers, T., De Waele, B., 2005. A review of the Mesoproterozoic to early Palaeozoic magmatic and tectonothermal history of south–central Africa: implications for Rodinia and Gondwana. J. Geol. Soc. 162 (3), 433–450.
Julia, J., Ammon, C.J., Herrmann, R.B., Correig, A.M., 2000. Joint inversion of receiver function and surface wave dispersion observations. Geophys. J. Int. 143 (1), 99–112.
Julia, J., Ammon, C.J., Nyblade, A.A., 2005. Evidence for mafic lower crust in Tanzania, East Africa, from joint inversion of receiver functions and Rayleigh wave dispersion velocities. Geophys. J. Int. 162 (2), 555–569.
Kachingwe, M., Nyblade, A., Julia, J., 2015. Crustal structure of Precambrian terranes in the southern African subcontinent with implications for secular variation in crustal genesis. Geophys. J. Int. 202 (1), 533–547.
Katongo, C., Koller, F., Kloetzli, U., Koeberl, C., Tembo, F., De Waele, B., 2004. Petrography, geo- chemistry, and geochronology of granitoid rocks in the Neoproterozoic-Paleozoic Lufilian–Zambezi belt, Zambia: implications for tectonic setting and regional correlation. J. Afr. Earth Sci. 40 (5), 219–244.
Kgaswane, E.M., Nyblade, A.A., Julia, J., Dirks, P.H.G.M., Durrheim, R.J., Pasyanos, M. E., 2009. Shear wave velocity structure of the lower crust in southern Africa: evidence for compositional heterogeneity within Archaean and Proterozoic terrains. J. Geophys. Res. Solid Earth 114 (B12). https://doi.org/10.1029/2008JB006217.
Kokonyangi, J., Armstrong, R., Kampunzu, A.B., Yoshida, M., Okudaira, T., 2004. U–Pb zircon geochronology and petrology of granitoids from Mitwaba (Katanga, Congo): implications for the evo- lution of the Mesoproterozoic Kibaran belt. Precambr. Res. 132 (1), 79–106.
Langston, C.A., 1979. Structure under Mount Rainier, Washington, inferred from teleseismic body waves. J. Geophys. Res. Solid Earth 84 (B9), 4749–4762.
Last, R.J., Nyblade, A.A., Langston, C.A., Owens, T.J., 1997. Crustal structure of the East African Plateau from receiver functions and Rayleigh wave phase velocities. J. Geophys. Res. Solid Earth 102, 24469–24483.
Lavreau, J., Deblond, A., 2000. Geological and chronological setting of the greenstone belts of the northern Congo Craton. J. Afr. Earth Sci. 30 (4), 53.
Lenoir, J.L., Liégeois, J.-P., Theunissen, K., Klerkx, J., 1994. The Palaeoproterozoic Ubendian shear belt in Tanzania: geochronology and structure. J. Afr. Earth Sci. 19 (3), 169–184.
Ligorria, J.P., Ammon, C.J., 1999. Iterative deconvolution and receiver-function estimation. Bull. Seismol. Soc. Am. 89 (5), 1395–1400.
Manya, S., Maboko, M.A.H., 2003. Dating basaltic volcanism in the neoarchaean sukumaland green- stone belt of the Tanzania craton using the Sm–Nd method: implications for the geological evolution of the Tanzania craton. Precambr. Res. 121 (1), 35–45.
Möller, A., Appel, P., Mezger, K., Schenk, V., 1995. Evidence for a 2 Ga subduction zone: eclogites in the Usagaran belt of Tanzania. Geology 23 (12), 1067–1070.
Muhongo, S., Lenoir, J.-L., 1994. Pan-African granulite-facies metamorphism in the Mozambique Belt of Tanzania: U-Pb zircon geochronology. J. Geol. Soc. 151 (2), 343–347.
Nguuri, T.K., Gore, J., James, D.E., Webb, S.J., Wright, C., Zengeni, T.G., Gwavava, O., Snoke, J.A., Group, K.S., 2001. Crustal structure beneath southern Africa and its implications for the formation and evolution of the Kaapvaal and Zimbabwe cratons. Geophys. Res. Lett. 28 (13), 2501–2504.
Nyblade, A., Dirks, P., Durrheim, R., Webb, S., Jones, M., Cooper, G., Graham, G., 2008. AfricaArray: developing a geosciences workforce for Africa's natural resource sector. Lead. Edge 27 (10), 1358–1361.
Nyblade, A.A., Durrheim, R., Dirks, P., Graham, G., Gibson, R., Webb, S., 2011. Geoscience initiative develops sustainable science in Africa. Eos, Transactions American Geophysical Union 92 (19), 161–162.
Nyblade, A., 2015. Data from: AfricaArray - Namibia. IRIS. https://doi.org/10.7914/SN/8A2015.
Nyblade, A., 2017. Data from: broadband seismic experiment in NE Uganda to investigate plume- lithosphere interactions. International Federation of Digital Seismograph Networks. https://doi.org/10.7914/SN/XW2017.
Ogden, C.S., Bastow, I.D., Ebinger, C., Ayele, A., Kounoudis, R., Musila, M., Bendick, R., Mariita, N., Kianji, G., Rooney, T., Sullivan, G., Kibret, B., 2023. The development of multiple phases of superposed rifting in the Turkana Depression, East Africa: evidence from receiver functions. Earth Planet Sci. Lett. 609, 118088. https://doi.org/10.1016/j.epsl.2023.118088.
Parra-Avila, L.A., Baratoux, L., Eglinger, A., Fiorentini, M.L., Block, S., 2019. The eburnean magmatic evolution across the baoul'e-mossi domain: geodynamic implications for the West African craton. Precambr. Res. 332, 105392.
Parra-Avila, L.A., Kemp, A.I.S., Fiorentini, M.L., Belousova, E., Baratoux, L., Block, S., Jessell, M., Bruguier, O., Begg, G.C., Miller, J., Davis, J., McCuaig, T.C., 2017. The geochronological evolution of the Paleoproterozoic Baoul'e-Mossi domain of the southern West African Craton. Precambr. Res. 300, 1–27.
Penaye, J., Toteu, S.F., Tchameni, R., Van Schmus, W.R., Tchakounté, J., Ganwa, A., Minyem, D., Nsifa, E.N., 2004. The 2.1 Ga West Central african belt in Cameroon: extension and evolution. J. Afr. Earth Sci. 39 (3), 159–164.
Penaye, J., Toteu, S.F., Van Schmus, W.R., Nzenti, J.-P., 1993. U-Pb and Sm-Nd preliminary geochronologic data on the Yaound'e series, Cameroon: re-interpretation of the granulitic rocks as the suture of a collision in the Central African belt. Comptes rendus de l'Académie des sciences. Série 2, Mécanique, Physique, Chimie, Sciences de l'univers, Sciences de la Terre 317 (6), 789–794.

Penn State University, 2004. Data from: AfricaArray. International Federation of Digital Seismograph Networks. https://doi.org/10.7914/SN/AF.
Pinna, P., Jourde, G., Calvez, J.Y., Mroz, J.M., Marques, J.M., 1993. The Mozambique Belt in northern Mozambique: Neoproterozoic (1100–850 Ma) crustal growth and tectogenesis, and superimposed Pan-African (800–550 Ma) tectonism. Precambr. Res. 62 (1), 1–59.
Plasman, M., Tiberi, C., Ebinger, C., Gautier, S., Albaric, J., Peyrat, S., Déverchère, J., Le Gall, B., Tarits, P., Roecker, S., Wambura, F., Muzuka, A., Mulibo, G., Mtelela, K., Msabi, M., Kianji, G., Hautot, S., Perrot, J., Gama, R., 2017. Lithospheric low-velocity zones associated with a magmatic segment of the Tanzanian Rift, East Africa. Geophys. J. Int. 210 (1), 465–481.
Porada, H., Berhorst, V., 2000. Towards a new understanding of the neoproterozoic-early paleozoic lufilian and northern Zambezi belts in Zambia and the democratic republic of Congo. J. Afr. Earth Sci. 30 (3), 727–771.
Raveloson, A., Nyblade, A., Fishwick, S., Mangongolo, A., Master, S., 2015. The upper mantle seis- mic velocity structure of South-Central Africa and the seismic architecture of Precambrian lithosphere beneath the Congo Basin. In: de Wit, M.J., Guillocheau, F., de Wit, M.J. (Eds.), The Geology and Resource Potential of the Congo Basin. Springer, pp. 3–18.
Ring, U., Kröner, A., Toulkeridis, T., 1997. Palaeoproterozoic granulite-facies metamorphism and granitoid intrusions in the Ubendian-Usagaran Orogen of northern Malawi, east-central Africa. Precambr. Res. 85 (1), 27–51.
Rudnick, R.L., Fountain, D.M., 1995. Nature and composition of the continental crust: a lower crustal perspective. Rev. Geophys. 33 (3), 267–309.
Rudnick, R.L., Gao, S., 2003. Composition of the continental crust. Treatise on Geochemistry 3, 659.
Sandvol, E., Seber, D., Calvert, A., Barazangi, M., 1998. Grid search modeling of receiver functions: implications for crustal structure in the Middle East and North Africa. J. Geophys. Res. Solid Earth 103 (B11), 26899–26917.
Shang, C.K., Satir, M., Siebel, W., Nsifa, E.N., Taubald, H., Liégeois, J.P., Tchoua, F.M., 2004. TTG magmatism in the Congo craton; a view from major and trace element geochemistry, Rb–Sr and Sm–Nd systematics: case of the Sangmelima region, Ntem complex, southern Cameroon. J. Afr. Earth Sci. 40 (1), 61–79.
Stankiewicz, J., de Wit, M.J., 2013. 3.5 billion years of reshaped Moho, southern Africa. Tectonophysics 609, 675–689.
Sun, M., Gao, S.S., Liu, K.H., Mickus, K., Fu, X., Yu, Y., 2021. Receiver function investigation of crustal structure in the Malawi and Luangwa rift zones and adjacent areas. Gondwana Res. 89, 168–176.
Tack, L., Liégeois, J.P., Deblond, A., Duchesne, J.C., 1994. Kibaran A-type granitoids and mafic rocks generated by two mantle sources in a late orogenic setting (Burundi). Precambr. Res. 68 (3), 323–356.
Tadjou, J.-M., Nouayou, R., Kamguia, J., Kande, H.L., Manguelle-Dicoum, E., 2009. Gravity analysis of the boundary between the Congo craton and the Pan-African belt of Cameroon. Aust. J. Earth Sci. 102 (1).
Tchameni, R., Mezger, K., Nsifa, N.E., Pouclet, A., 2001. Crustal origin of early proterozoic syenites in the Congo craton (Ntem complex), South Cameroon. Lithos 57 (1), 23–42.
Thompson, D.A., Bastow, I.D., Helffrich, G., Kendall, J.-M., Wookey, J., Snyder, D.B., Eaton, D.W., 2010. Precambrian crustal evolution: seismic constraints from the Canadian Shield. Earth Planet Sci. Lett. 297 (3), 655–666.
Tokam, A.-P.K., Tabod, C.T., Nyblade, A.A., Julia, J., Wiens, D.A., Pasyanos, M.E., 2010. Struc- ture of the crust beneath Cameroon, West Africa, from the joint inversion of Rayleigh wave group velocities and receiver functions. Geophys. J. Int. 183 (2), 1061–1076.
Toteu, S.F., Penaye, J., Djomani, Y.P., 2004. Geodynamic evolution of the Pan-African belt in central Africa with special reference to Cameroon. Can. J. Earth Sci. 41 (1), 73–85.
Toteu, S.F., Van Schmus, W.R., Penaye, J., Michard, A., 2001. New U–Pb and Sm–Nd data from north-central Cameroon and its bearing on the pre-Pan African history of central Africa. Precambr. Res. 108 (1), 45–73.
Toteu, S.F., Van Schmus, W.R., Penaye, J., Nyobe, J.B., 1994. U–Pb and Sm–N evidence for Eburnian and Pan-African high-grade metamorphism in cratonic rocks of southern Cameroon. Precambr. Res. 67 (3), 321–347.
Treloar, P.J., Coward, M.P., Harris, N.B.W., 1992. Himalayan-Tibetan analogies for the evolution of the Zimbabwe craton and Limpopo belt. Precambr. Res. 55 (1), 571–587.
Trompette, R., 1994. Geology of Western Gondwana (2000 - 500 Ma): Pan-African-Brasiliano Aggregation of South America and Africa. CRC Press.
Tugume, F., Nyblade, A., Julia, J., 2012. Moho depths and Poisson's ratios of precambrian crust in east Africa: evidence for similarities in archean and proterozoic crustal structure. Earth Planet Sci. Lett. 355–6, 73–81.
Tugume, F., Nyblade, A., Julia, J., van der Meijde, M., 2013. Precambrian crustal structure in Africa and Arabia: evidence lacking for secular variation. Tectonophysics 609, 250–266.
Wang, T., Gao, S.S., Yang, Q., Chen, L., Liu, K.H., 2022. Lithospheric structure underneath the Archean Tanzania Craton and adjacent regions from a joint inversion of receiver functions and Rayleigh-wave phase velocity dispersion. Seismol Res. Lett. 93 (3), 1753–1767. https://doi.org/10.1785/0220210296.
Walraven, F., Rumvegeri, B.T., 1993. Implications of whole-rock Pb–Pb and zircon evaporation dates for the early metamorphic history of the Kasaı craton, Southern Zaıre. Journal of African Earth Sci- ences (and the Middle East) 16 (4), 395–404.
Webb, S., Manzi, M., Scheiber-Enslin, S., Chinamora, B., Naidoo, A., Lee, S.A., Isiaka, A., Mngadi, S., Tshitlho, K., Nyblade, A., Emry, E., 2015. AfricaArray international geophysics field school: diversity and training come together in Africa. Lead. Edge 34 (10), 1230–1235.
Wölbern, I., Rümpker, G., Schumann, A., Muwanga, A., 2010. Crustal thinning beneath the Rwenzori region, Albertine rift, Uganda, from receiver-function analysis. Int. J. Earth Sci. 99 (7), 1545–1557.
Wright, J.B., Hastings, D.A., Jones, W.B., Williams, H.R., 1985. Geology and Mineral Resources of West Africa. Springer, Netherlands, pp. 56–69.
Wysession, M., Wiens, D., Nyblade, A., 2015. Data from: investigation of sources of intraplate volcanism using passcal broadband Instruments in Madagascar, the comores, and Mozambique. International Federation of Digital Seismograph Networks. https://doi.org/10.7914/SN/XV2011.
Young, A.J., 2012. Crustal Structure of Southestern Tanzania. Penn State University.
Youssof, M., Thybo, H., Artemieva, I.M., Levander, A., 2013. Moho depth and crustal composition in Southern Africa. Tectonophysics 609, 267–287.
Yu, Y., Liu, K.H., Reed, C.A., Moidaki, M., Mickus, K., Atekwana, E.A., Gao, S.S., 2015. A joint receiver function and gravity study of crustal structure beneath the incipient Okavango Rift, Botswana. Geophys. Res. Lett. 42 (20), 8398–8405.
Zandt, G., Ammon, C.J., 1995. Continental crust composition constrained by measurements of crustal Poisson's ratio. Nature 374 (6518), 152–154.
Zhu, L., Kanamori, H., 2000. Moho depth variation in southern California from teleseismic receiver functions. J. Geophys. Res. Solid Earth 105 (B2), 2969–2980.